STRUCTURE AND GEOMETRY OF THE EUREKA VALLEY EXTENSIONAL BASIN, EASTERN CALIFORNIA, FROM GRAVITY MODELING

by

Lauren Ashley Landreneau

APPROVED BY SUPERVISORY COMMITTEE:

_____

John F. Ferguson, Chair

_____

John W. Geissman

_____

Carlos L. V. Aiken

To my father, who let me eat chocolate cake for breakfast.

STRUCTURE AND GEOMETRY OF THE EUREKA VALLEY EXTENSIONAL BASIN, EASTERN CALIFORNIA, FROM GRAVITY MODELING

by

LAUREN ASHLEY LANDRENEAU, BS

THESIS

Presented to the Faculty of

The University of Texas at Dallas

in Partial Fulfillment

of the Requirements

for the Degree of

MASTER OF SCIENCE IN

GEOSCIENCES

THE UNIVERSITY OF TEXAS AT DALLAS

May 2019

ACKNOWLEDGMENTS

I would like to thank my advisor, John Ferguson, for his support and guidance in this research. I would also like to thank my committee members, John Geissman and Carlos Aiken, for going above and beyond in guiding me along the way. I would also like to thank John Oldow for his assistance in the field and participating early on in this research.

I am also grateful to Sarah Sokol, Nick Mueller, and August Ridde for their assistance in the field. The endless support, collaboration and encouragement I have received from Sarah Sokol will be forever appreciated. I would also like to thank the UTD Department of Geosciences for their support; they have encouraged me to pursue this research and imparted their expert advice throughout this project.

This work was supported by Pioneer Natural Resources and The University of Texas at Dallas.

December 2018

STRUCTURE AND GEOMETRY OF THE EUREKA VALLEY EXTENSIONAL BASIN, EASTERN CALIFORNIA, FROM GRAVITY MODELING

Lauren Ashley Landreneau, MS
The University of Texas at Dallas, 2019

Supervising Professor: John F. Ferguson

Eureka Valley, situated in eastern California, is a north-northwest trending extensional basin characterized by northeast striking, northwest dipping normal faults that serve to displace offset from the Hunter Mountain – Panamint Valley – Saline Valley fault system to the Death Valley – Furnace Creek – Fish Lake Valley fault system. To evaluate the subsurface geometry of Eureka Valley a detailed relative gravity survey was conducted and a residual complete Bouguer anomaly map was produced and inverted for depth. Geologic cross-sections and a fault model were used to forward model the gravity data. A fault displacement budget, with respect to the extension direction, allows for the trigonometric determination within the basin. Estimated minimum vertical displacements range between 3.8 and 4.1 km were based on restoring basement depths to a pre-extensional datum. Using the regional extension direction of N65W and a fault dip of 60˚, we calculated an aggregate horizontal extension of 4 km across Eureka Valley. With extension starting after 4 Ma, the average displacement rate is 1.0 mm/yr.

TABLE OF CONTENTS

ACKNOWLEDGMENTS v

ABSTRACT vi

LIST OF FIGURES ix

LIST OF TABLES x

CHAPTER 1 INTRODUCTION 1

CHAPTER 2 REGIONAL TECTONIC FRAMEWORK 3

CHAPTER 3 STRUCTURE AND STRATIGRAPHY OF EUREKA VALLEY 7

3.1 Physiography 7

3.2 Fault Geometry 9

3.3 Stratigraphy 10

CHAPTER 4 SUBSURFACE BASIN MORPHOLOGY 14

4.1 Gravity Methods 14

4.2 Depth Inversion 21

4.3 Subsurface Morphology 26

4.4 2D Forward Models 28

CHAPTER 5 FAULT MODEL AND DISPLACEMENT BUDGET 41

5.1 Fault Model 41

5.2 Displacement Component Determination 44

5.3 Displacement Budget 47

CHAPTER 6 DISCUSSION AND CONCLUSION 51

REFERENCES 53

BIOGRAPHICAL SKETCH 58

CURRICULUM VITAE 59

LIST OF FIGURES

Figure 2.1 Regional physiographic map of the northern Eastern California Shear Zone.....4

Figure 3.1 Eureka Valley and vicinity physiographic markers.....8

Figure 3.2 Geologic map of Eureka Valley and the surrounding highlands.....11

Figure 4.1 Spatial distribution of gravity stations collected in Eureka Valley.....15

Figure 4.2 Regional Bouguer gravity map.....17

Figure 4.3 Bouguer anomaly gravity map of Eureka Valley area.....19

Figure 4.4 Residual Bouguer anomaly map of Eureka Valley.....20

Figure 4.5a Isopach map of basin fill sediments produced by depth inversion models.....24

Figure 4.5b Isopach map of basin fill sediments produced by depth inversion models.....25

Figure 4.6 Structural domains of Eureka Valley.....27

Figure 4.7 Geologic map of Eureka Valley with cross section for 2D profiles.....30

Figure 4.8 Two-dimensional geophysical model profiles.....35

Figure 4.9 Fence diagrams of two-dimensional profiles.....40

Figure 5.1 Fault map of Eureka Valley with vertical displacements.....43

Figure 5.2 Fault map of Eureka Valley with horizontal extension.....47

Figure 5.3 Fault displacement components.....48

Figure 5.4 Simplified estimated of horizontal extension for both domains.....50

LIST OF TABLES

Table 4.1 Depth-density values used in the inversion modeling 22

Table 4.2 Lithologic units used in 2D forward models 31

CHAPTER 1

INTRODUCTION

In zones of transtensional deformation in continental lithosphere, systems of normal and strike-slip faults are kinematically coordinated and allow for the transfer of displacement from one active fault system to another (Burchfiel et al., 1987; Oldow, 1992; Mouslopoulou et al., 2007). Transtensional deformation within the Eastern California shear zone is accommodated by active systems of strike-slip and dip-slip faults. Displacement transfer between sub-parallel strike-slip faults is facilitated by extension on kinematically linked dip-slip faults and results in the opening of deep transtensional basins. Within this system, it is possible to determine the spatial distribution and kinematic associations of faults, and quantify the magnitude of extension and right-lateral displacement accommodated.

Eureka Valley is north-northwest trending basin that formed in response to displacement transfer between two of the strike-slip fault systems in the ECSZ, the Panamint Valley – Hunter Mountain –Saline Valley and Furnace Creek – Fish Lake Valley fault systems in the last 3 to 4 Ma from the late Pliocene (Burchfiel, 1987, Dixon et al., 2000). The basin is characterized by dip-slip dominated faults that serve as a mechanism by which displacement is transferred north to the Furnace Creek – Fish Lake Valley fault system. To determine the magnitude of displacement for this structurally complex system, a geophysical imaging study was completed. In addition, construction of a fault model of basin and range-bounding faults provides a means to examine the displacement budget for the system. This thesis explores the magnitude of net displacement that was accommodated by the faults within and bounding Eureka Valley since its

opening and aims to quantify the amount of right-lateral displacement that has been transferred through structures in Eureka Valley.

CHAPTER 2

REGIONAL GEOLOGIC FRAMEWORK

The Eastern California Shear Zone (ECSZ; Dokka and Travis, 1990) and Central Walker Lane (Oldow, 1992) constitute an active tectonic belt of intracontinental deformation that has localized about 25% of the total relative motion between the Pacific and North American plate (Argus and Gordon, 1991; Dixon et al., 2000; Bennett et al., 2003). This tectonic boundary zone accommodates contemporary differential displacement between the northwest translating Sierra Nevada and the west-northwest extending Basin and Range and is characterized by large magnitude right-lateral shear and extension (Oldow, 1992, 2003; Dixon et al., 2000, Bennett et al., 2003). Transtensional deformation in the region began about 5 or 3 Ma (Oldow, 1992; Oldow et al., 2008; Stockli et al., 2003; Lee et al., 2009) and an extension direction of N65W from the mid-Pliocene to present is recorded by GPS velocities, fault slip inversion and earthquake focal mechanisms (Dixon et al., 2000; Oldow et al., 2003).

Displacement within the northern ECSZ (Figure 2.1) is transferred between three main sub-parallel northwest striking fault systems, from west to east, Owens Valley – White Mountain (OV-WM), Saline Valley – Hunter Mountain – Panamint Valley (PV – HM – SV), Death Valley – Furnace Creek – Fish Lake Valley (DV-FC-FLV) fault systems (Reheis and Dixon, 1996; Frankel et al., 2007a). These major faults transfer right-lateral oblique displacement to the east, from south to north, by a series of northeast trending, normal faults (Reheis and Dixon, 1996). In the north, the Deep Springs fault zone transfers ~15-65% of displacement from the OV – WM fault system to the DV – FC – FLV system. Sokol (2019) determined a slip rate of 0.7 mm/yr on the Deep Springs fault system which aligns with extension rates of 0.2-0.7 mm/yr determined by

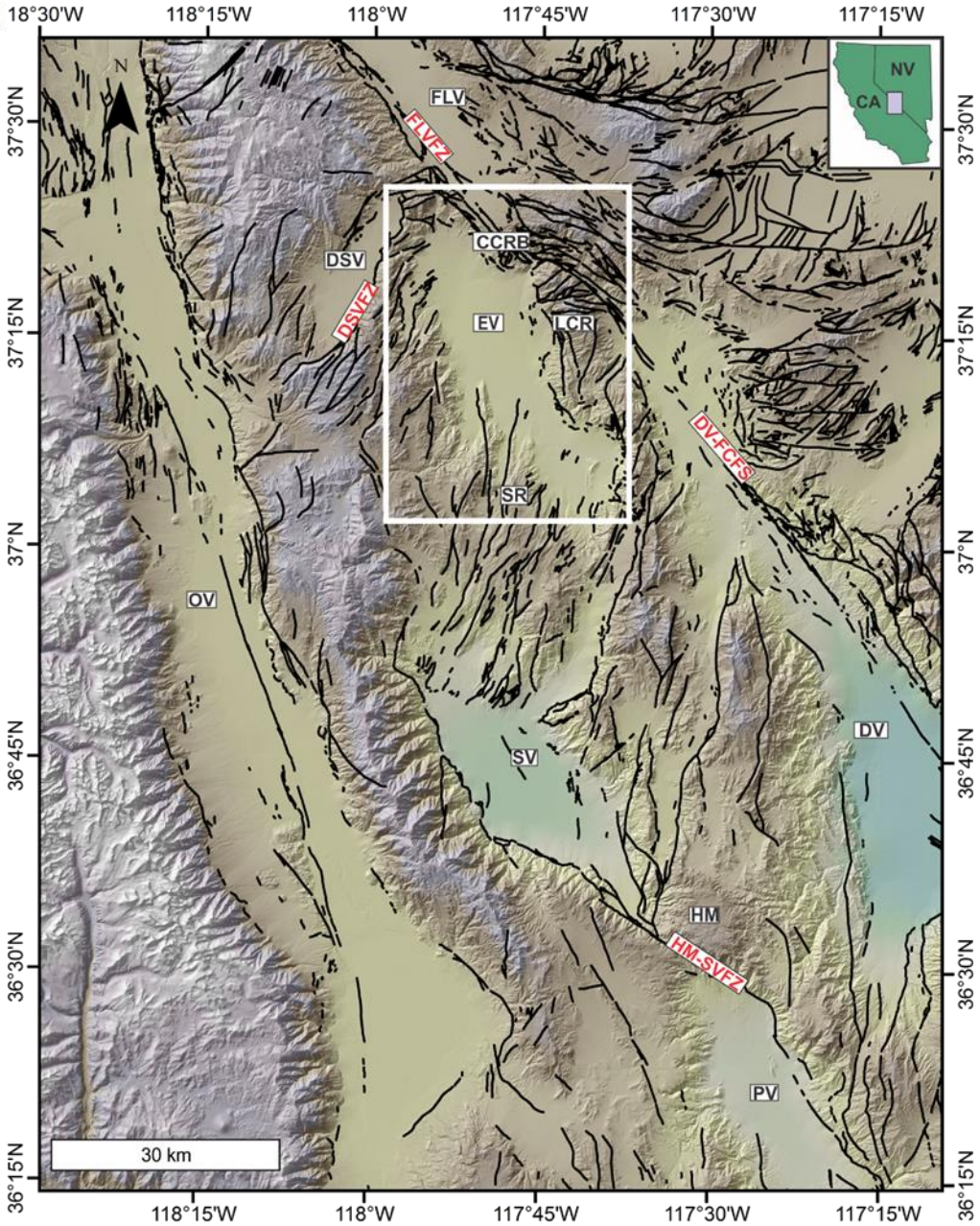

Figure 2.1. Shaded relief map of the northern Eastern California Shear Zone, displaying fault traces in black. Physiographic locations are labeled in black and major fault systems are labeled in red. EV – Eureka Valley, SV – Saline Valley, DSV – Deep Springs Valley, PV – Panamint Valley, DV – Death Valley, OV – Owens Valley, FLV – Fish Lake Valley, HM – Hunter Mountain, CCRB – Cucomonga Canyon Restraining Bend , LCR – Last Chance Range, SR Saline Range, DV-FCFZ – Death Valley-Furnace Creek Fault Zone, DSVFZ – Deep Springs Valley Fault Zone, FLVFZ – Fish Lake Valley Fault Zone, HM-SVFZ – Hunter Mountain-Saline Valley Fault Zone, OVFZ – Owens Valley Fault Zone.

Lee et al. (2001). To the south, three strands of faults actively transfer displacement east out of Saline Valley; the Cottonwood and Dry Mountain fault systems transfer displacement directly to the Furnace Creek fault system in Death Valley and the northern most strand transfers displacement via a complex array of northeast-trending dip-slip faults cutting basalts in the Saline Range. The magnitude and distribution of present-day dextral displacement among these predominantly strike-slip fault zones in the northern Eastern California Shear Zone vary significantly spatially and temporally.

The northwest striking, right-oblique Panamint Valley-Hunter Mountain-Saline Valley fault system (PV-HM-SVFZ) lies ~45 km to the southwest of the Death Valley – Furnace Creek – Fish Lake Valley fault system and extends about 150 km from its termination at the Garlock fault north to Saline Valley, bounding the east side of the Inyo Mountains. Saline Valley and Panamint Valley fault systems are dominated by northwest striking normal faults and are kinematically linked to form a complex interaction with the predominantly strike-slip Hunter Mountain fault zone (Burchfiel, 1987; Oswald and Wesnousky, 2001; Gourmelen, 2010; Lee, 2009). Inception of the HM-SV-PV fault system is bracketed between 2.8 +/- 0.7 Ma with the rapid exhumation of the bounding Inyo Mountains (Lee et al., 2009a), and 4.0 Ma from Pliocene basalt offsets (Burchfiel, 1987). Right-lateral displacement estimates for this fault zone ranges from 8 to10 km, along with 0-2 km of dip-slip movement through a series of normal faults that were based on offsets of ~4 Ma basalts overlying the Hunter Mountain Batholith (Burchfiel et al., 1987). Burchfiel et al. (1987) used maximum ages of 4 Ma dated on Pliocene basalt offset dated in the southern end of Saline Valley for the beginning of extension and strike-slip deformation on the Hunter Mountain – Saline Valley – Panamint Valley fault system. Sternlof

(1988) calculated long term slip rates of 3.2-3.4 mm/yr for the region north of Saline Valley assuming extension began at 1.7 Ma. These faults continue north into Eureka Valley and accommodate displacement through a complex oblique-normal transfer system.

Eureka Valley is located to the south of the Death Valley – Furnace Creek – Fish Lake Valley fault zone, and to the northeast of the Panamint Valley – Hunter Mountain – Saline Valley fault system in eastern California. Eureka Valley is bound and kinematically linked to the southwest by the Saline Range (Figure 2.1) and displacement on north-northeast structures is locally transferred to high-angle structures within and bounding Eureka Valley. The northeast-trending normal faults that cut the basalts in the Saline Range continue northeast into Eureka Valley and cross the basin on the eastern margin north toward the Death Valley – Furnace Creek – Fish Lake Valley fault system. Larson (1979) dated basaltic volcanic flows in the Saline Range to infer that extension in the Saline Valley region has been active since 3.1 Ma. Sternlof (1988) argued for two periods of volcanic activity and extension in the Saline Range; one prior to 3 Ma and another between 1.7 and 1.4 Ma. Using 1.4 Ma as a timing constraint, Sternlof (1988) calculated about 4.5 +/- 0.6 km of extension resulting in an average strain rate of 2.8 to 3.6 mm/yr. Structures associated with this region are currently active, based on a remote sensing SAR interferometry study conducted on the May 17, 1994 M 6.1 earthquake in Eureka Valley (Pultzer and Rosen, 1995) and displacement of fluvial terraces associated with normal faults within Eureka Valley (Lawson, 2017).

CHAPTER 3

STRUCTURE AND STRATIGRAPHY OF EUREKA VALLEY

3.1 Physiography

Eureka Valley (Figure 3.1) is a topographic depression located to the south of the Death Valley – Furnace Creek – Fish Lake Valley fault zone, and to the northeast of the Panamint Valley – Hunter Mountain – Saline Valley fault system in eastern California. The elongated north-northwest trending basin is 45 km long and 12-17 km wide and is bounded on all sides by mountain ranges. The elevation of the valley floor decreases from northeast to southwest from about 1300 m to 890 m, surrounded by highlands with elevation ranging from 1400-2577 m. Elevation differences between the valley surface and adjacent topographic highs range from 200 to 1050 m. Three major topographic ridges line the western border of Eureka Valley and separate them from the main basin by ridges up to ~1200 m in elevation. Pediment surfaces separate the surrounding highlands from the valley floor and are lined by alluvial fans that encompass 83 percent of the valley floor (Blair, 2003) that derive from a catchment area between the nearby Sylvania Mountains.

The highlands surrounding Eureka Valley consist of the northern Inyo Mountains, Horse Thief Hills, and the Last Chance Range to the west, northwest and east, respectively and by the Saline Range to the southwest. In the northwest, the most prominent topographic high is Chocolate Mountain with a maximum elevation of 2240 m capped by Miocene basalt overlain unconformably on the Jurassic monzonites of Joshua Flat. Farther south, along the western bounding Inyo Mountains is Mount Nunn, at 2387 m, composed of Jurassic monzonite rocks of

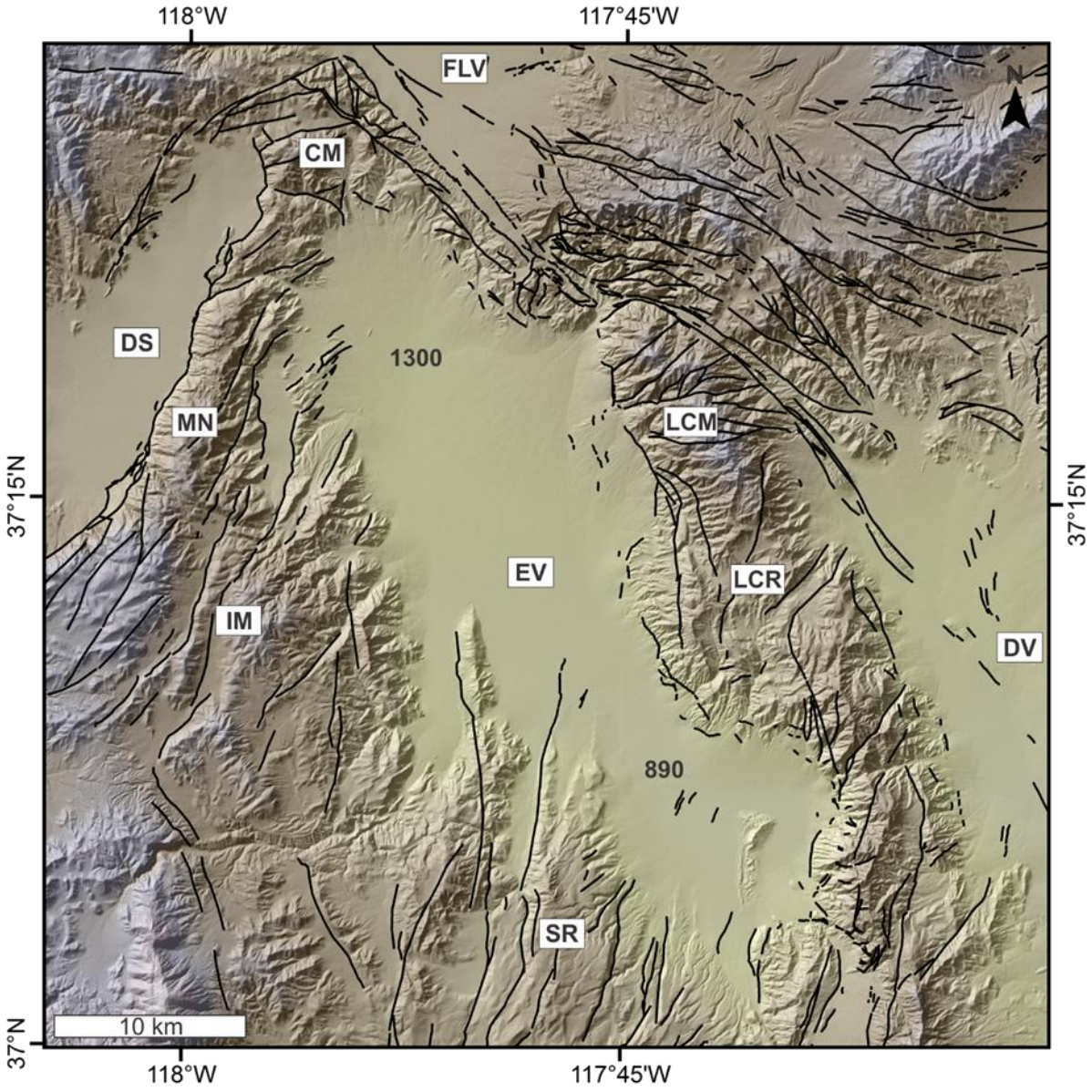

Figure 3.1. Eureka Valley and the surrounding regions showing fault regions and elevation in black. DS- Deep Springs; FLV- Fish Lake Valley; DV- Death Valley; CM- Chocolate Mountain; LCM- Last Chance Mountain; LCR- Last Chance Range; SR- Saline Range; IM- Inyo Mountains; MN- Mount Nunn.

Joshua Flat pluton. The Saline Range along the southwest of Eureka Valley trends northeast and has a maximum elevation of 2115 m at Saline Peak in the southwest closer to Saline Valley. The north-south trending Last Chance Range encompasses the eastern margin of the valley and extending north of the valley what is informally called Horse Thief Hills. Last Chance Mountain is the most prominent topographic high at 2577 m in the far northeast of the mapping area composed of Bonanza King Dolomite of the upper and middle Cambrian (McKee, 1968). Dry Mountain south of Eureka Valley, is the most prominent topographic high in the Last Chance Range at 2644 m.

3.2 Fault Geometry

Eureka Valley is separated from the bounding ranges by an active array of linked north-northwest to north-east normal to oblique-slip faults. Faults that separate the range from the valley are not parallel and display a distinct change in orientation. The east is defined by a high-angle north-northwest trending fault the trace of which is at the range front of the Last Chance Range. The western boundary of Eureka Valley is more irregular than the east and is controlled by northeast to north-west normal faults that form major topographic ridges in the west. The fault map illustrates a change in orientation from northeast trending faults stretching across the basin and merging with north-northwest trending faults on the east side of the basin.

In the northwest, basin bounding faults are north-northeast striking normal faults dipping southeast, with N45E average orientation that run parallel to the Deep Springs fault zone and enter Eureka Valley. The 10 km wide fault zone includes 3-4 major strands, with locally interrelated shorter strands that can be traced nearly 21 km along strike from the southwest at the boundary of Owens Valley in the Inyo Mountains to the Horse Thief Hills in the northwest.

North of Mount Nunn, a strand of the Deep Springs fault zone splays off of the main trajectory and heads east-northeast through Solider Pass into the northwest corner of Eureka Valley. The eastern boundary of Eureka Valley is controlled by the north-northwest curvilinear fault that serves as a structural boundary between the Last Chance Range and Eureka Valley. The north-northwest high angled oblique fault is mapped for 25-30 km and separates basin fill and bedrock, and is associated with fault scarps 1-5 meters high.

The highlands to the south and west of Eureka Valley are dissected by a distributed array of north-northeast to north-south trending extensional faults. The north-northeast array of faults stretches nearly 70 km in width from the southeast to the northwest, and internally dismember the region situated between the northern Cottonwood Mountains and northern Inyo Mountains. Individual north-northeast trending faults display trace lengths that range from several kilometers to up to 50 km, with average lengths of 20-30 km and form these major topographic ridges. The May 17th, 1993, M_W= 6.1 Eureka Valley earthquake activated a north-northeast striking normal fault on a large escarpment in the Saline Range (Peltzer and Rosen, 1995) and that the region is still currently active. The north-northeast array of faults have individual spacings between strands of a few hundred meters to up to 7 km, and kinematically link the two major dextral fault systems.

3.3 Stratigraphy

The topography surrounding Eureka Valley (Figure 3.2) consists of Proterozoic to Paleozoic carbonate and siliciclastic meta-sedimentary rocks intruded by Mesozoic quartz monzonites overlain unconformably by upper Cenozoic volcanic and sedimentary rocks (McKee and Nelson, 1967; McKee, 1968; Reheis and Sawyer, 1997). The most common rock type in the mountains

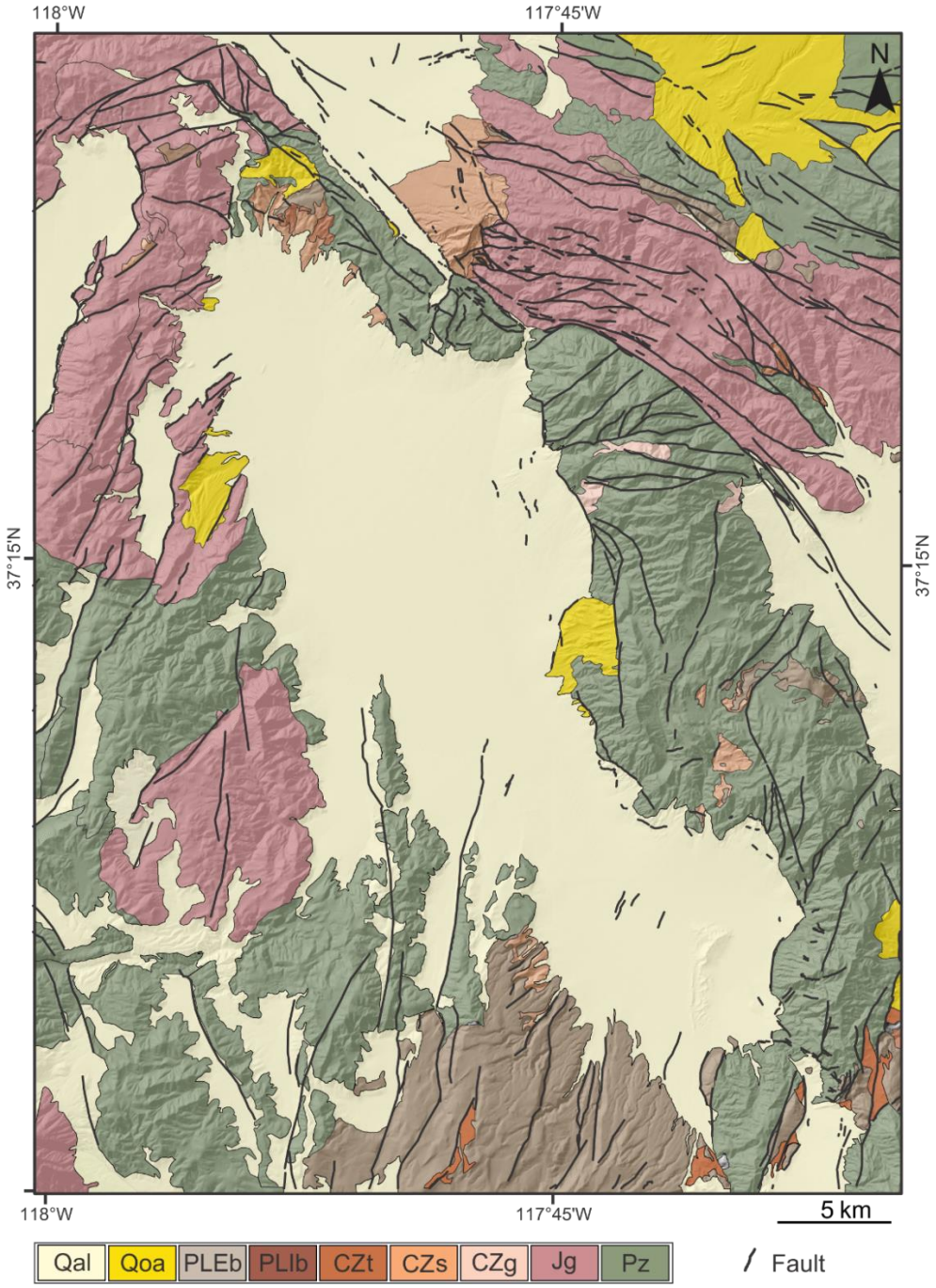

Figure 3.2. Geologic map of Eureka Valley. Units: Pz-Proterozoic to Paleozoic metasedimentary rocks, Jg- Jurassic and Cretaceous monzonites; CZg- Miocene monzonites; CZs- Cenozoic sandstone; CZt- Cenozoic rhyolitic tuff; PLIb- Pliocene basalt; PLEb-Pleistocene basalt; Qoa-Quaternary alluvial fan and fluvial deposits; Qal- Quaternary alluvium and valley-fill deposits

surrounding the valley are the Proterozoic to Paleozoic carbonate and siliclastic rocks exposed in each region of the mapping area. The Proterozoic and Paleozoic strata have an aggregate thickness of at least 15 km, and are composed of dolomite, shale, and limestone that have been heavily faulted and folded (Hunt and Mabey, 1966; Nelson, 1978). Deep Springs Ridge and north of Marble Canyon expose Jurassic quartz monzonites of Beer Creek and Jurassic hornblende-augite monzonites of Joshua Flat, respectively and range in age from 175 to 85 Ma (McKee and Nelson, 1967; McKee, 1985). The Beer Creek monzonite is also exposed to the northeast of the Last Chance Range in the Sylvania Mountains.

Cenozoic volcanic deposits around the basin vary in age, thickness, lithology, and stratigraphic sequence and are limited to the south and the extreme northwest extent of Eureka Valley and rest unconformably on Pre-Cenozoic rocks. In the north, exposed west of Horse Thief Canyon, middle Miocene to Pliocene basalt, rhyolitic ash-flow tuff, and sedimentary rocks over 450 meters thick sit unconformably above Paleozoic basement rocks (Reheis and McKee, 1991; Reheis, 1992; Reheis and Sawyer, 1997). Late Miocene basalt and the rhyolitic tuff tops Chocolate Mountain and is dated at 11.5 to 10.8 Ma (Dalrymple, 63). Similar ages were determined by Mueller (2017) using 40Ar/39Ar geochronology on basalt flows of 11.6 +/- 0.03 Ma in the Horse Thief Hills. North of Last Chance Mountain, exposures of Miocene granitic rocks of the Last Change range appear as small stocks that flank the west and east of the range (McKee, 1968). The most abundant exposures of upper Cenozoic volcanics and sedimentary rocks are located in the Saline Range and the adjacent Last Chance Range. The Cenozoic section in the southern part of Eureka Valley is dominated by thick exposures of Pliocene basalt with minor accumulations of underlying sedimentary rocks that unconformably overlie Paleozoic

basement rocks restricted to the Saline Range and can be laterally traced for 10's of kilometers. Outcrops of 3.5 to 1.4 Ma basalts lie on Paleozoic metasedimentary basement rocks and include rare outcrops of ash-rich sedimentary rocks and tuffs of unknown age (Ross, 1970; Larson, 1979; Sternlof, 1988). Thickness estimates of volcanic rocks in the Saline Range by Blakely and McKee (1985) are around 1000 m, but Sternlof (1988) states the average thickness is around 500 meters. The variation in the Cenozoic sequences surrounding Eureka Valley could reflect different volcanic origins, distribution of late Cenozoic deformation and nonplanar topography, which would hinder lateral continuity as well as preservation.

CHAPTER 4

SUBSURFACE BASIN MORPHOLOGY

4.1 Gravity Methods

To evaluate the subsurface geometry of Eureka Valley a detailed relative gravity survey was conducted and a residual Bouguer gravity anomaly map was produced. Prior to this study, data coverage of the basin, provided by the Pan American Center of Earth Studies (PACES), was limited to 40 stations within Eureka Valley. To ensure adequate coverage, an additional 529 stations were collected (Figure 4.1) at a nominal station spacing of 300 meters along four east-west trending transects and several secondary paths. Access was limited due to proximity of Death Valley National Park, transects followed paths available within the park and others acquired by traversing on foot. The east-west trending transects begin and end in bedrock, all other transects cross-cut at least one of these east-west trending transects to generate a grid of data and do not always begin and end in bedrock due to limited access along paths. Gravity stations were reoccupied every 1.5 km along a northeast trending transect in the far north with both gravimeters used to reoccupy several PACES stations throughout the survey to verify internal consistency of data.

Data were collected using two CG-5 Autograv gravimeters, three Leica Viva dual frequency Global Navigation Satellite System (GNSS) units, and two 4x4 all-terrain vehicles. The CG-5 gravimeter averages sensor output over 60 seconds for each meter reading. At each station three, sometimes four, readings were collected to identify any variations in the measurements. GNSS positions for all gravity stations were referenced to two base stations, one within the basin and one located northeast in Dyer, Nevada, and occupied with both

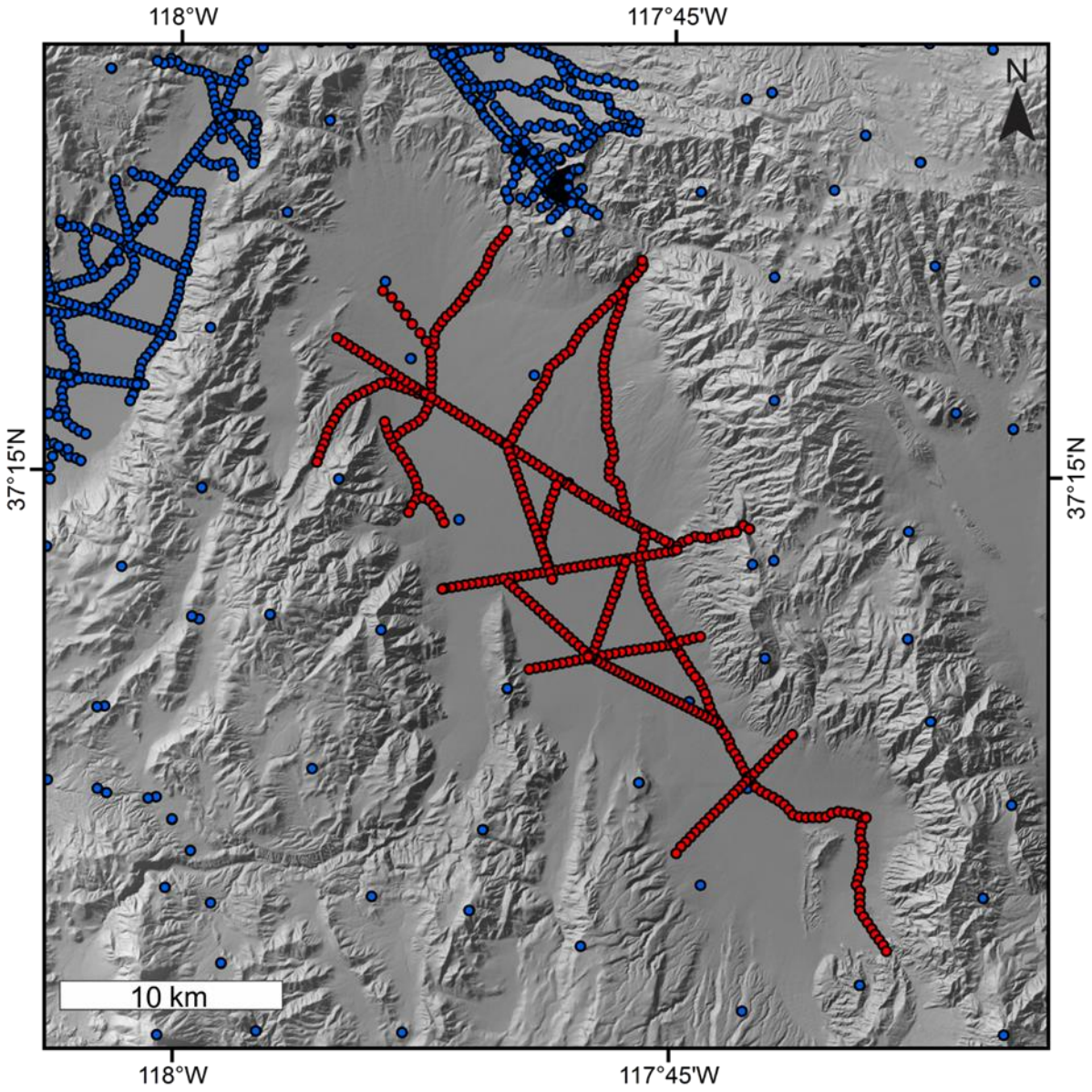

Figure 4.1. Spatial distribution of gravity stations acquired by students The University of Texas at Dallas during the summer of 2017 (red), stations previously collected by students of The University of Texas at Dallas and stations obtained by the Pan American Center for Earth and Environmental Studies (blue).

gravimeters at the beginning and ending of each day to obtain a closed loop. GNSS positions were collected in real-time kinematic acquisition, providing a positioning of 2.5 cm or better, and post processed using Leica GeoOffice software. Location of the base station was determined using the Continuously Operating Reference Stations network via the Online Positioning User Service (OPUS) provided by the National Geodetic Survey (NGS). All the data were post processed in reference to the OPUS corrected base station using Leica GeoOffice software. The base station within the basin is located at 37˚14'54.13", -117˚48'26.57" and has a mean elevation of 1015.98 +/- 0.0016 m with a minimum of 91% of observations used and ambiguities fixed and a maximum uncertainty of 1.3 cm.

A Bouguer gravity map was computed for Eureka Valley (Figure 4.2). Gravity data were terrain corrected using the 2011 "grav proc" MatLab program developed by Dr. John Ferguson at The University of Texas at Dallas in accordance with standards set by the USGS (Hildenbrand et al., 2002). Terrain corrections for the inner (Cogbill, 1989) and outer (Plouff, 1966) applied 1/3 arc-second, 10 m DEM data and a 1 arc-second, 30 m DEM data, respectively, as obtained from The National Map provided by the USGS National Geospatial Program. In order to construct a Bouguer gravity map of the region, the gravity data from this survey were merged with ~3500 gravity measurements collected by previous UTD students between 2012 and 2017, along with measurements within 170 km radius of Eureka Valley provided by PACES, for a total of about 80,000 gravity measurements. The Bouguer gravity map was calculated using the spreadsheet of Holom and Oldow (2007) in conformity with standards set forth by the U.S. Geological Survey (Hildenbrand et al., 2002) and the Standards/Format Working Group of the North American Gravity Database Committee (Hinze, 2003) with a reduction density of 2.67 g/cm^3. The Bouguer

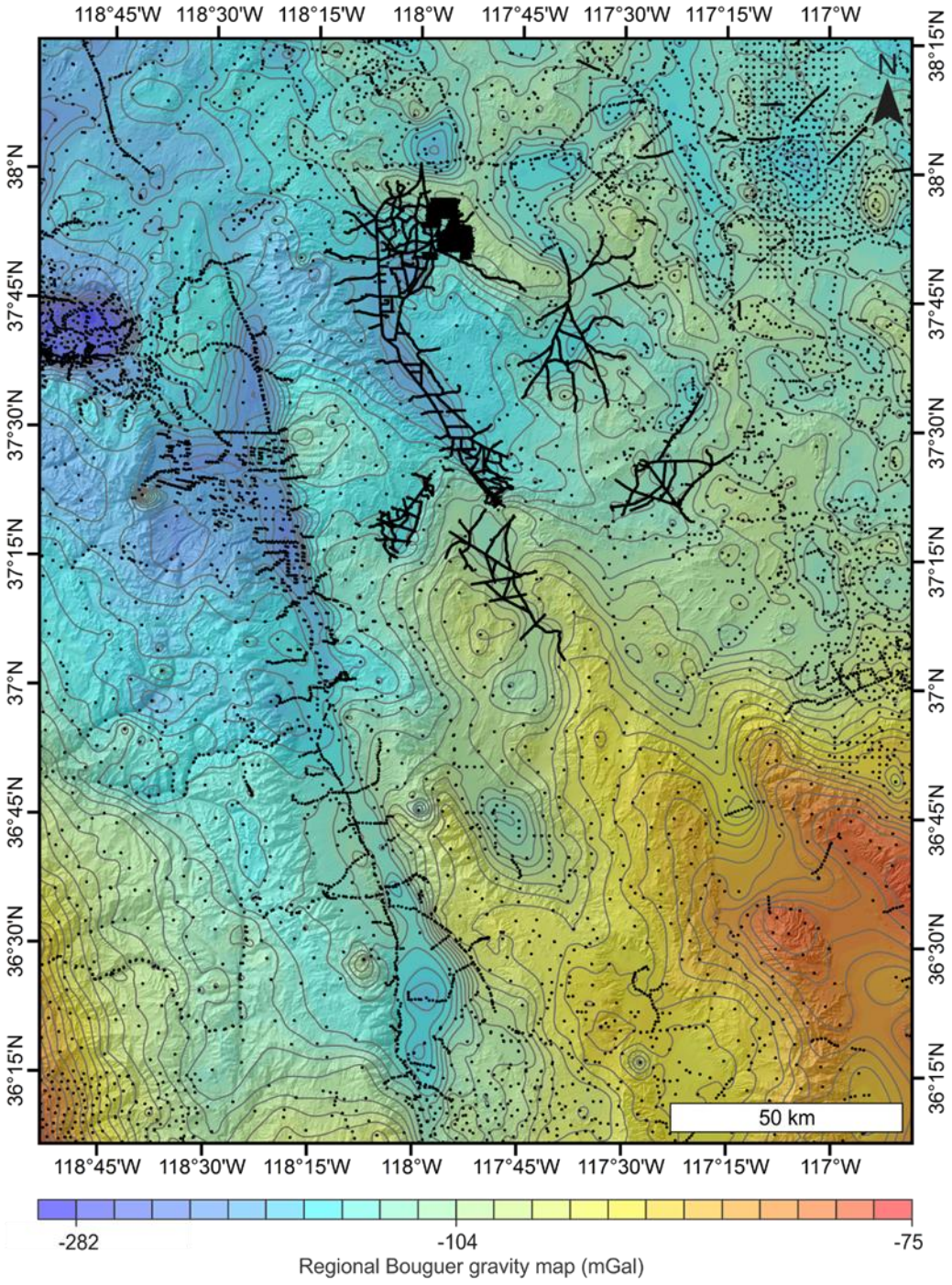

Figure 4.2. Complete Bouguer gravity map of Eureka Valley and surrounding environments illustrating regional features. Gravity stations are shown in black.

gravity map illustrates regionally where the more prominent regional structures are located and identifies local density anomalies. The location and thickness of Cenozoic volcanic rocks contribute to the gravity anomalies and illustrates major faults that have been essential in the Cenozoic evolution of these basins. In the southwest, a regional northwest trending ridge can be seen encompassing Death Valley to the Eureka Valley area. In the vicinity of Eureka Valley and Deep Springs Valley the gravity is relatively flat, with values ranging a few mGals but remaining fairly constant. Owens Valley and southern Fish Lake Valley, to the west and north respectively, exhibit gravity lows that correspond to the underlying deep basins. Surrounding Eureka Valley (Figure 4.3), a relative high of -160 mGal in the east associated with the Last Chance Range and two gravity lows with values -220 and -230 mGal to the north associated with Deep Springs Valley and southern Fish Lake Valley, respectively. In Eureka Valley, local anomalies (Figure 4.3) are present in the north with a low of -196 mGal, and in the south with a value of -183 mGal. The southern gravity low is bounded and separated from the north by a relative northeast trending gravity high, -175 mGal, associated with mapped faults. Where some ambiguity lies is in the Saline Range to the south, where a gravity low of -193 mGal is dominated by thick deposits of basalt and would be expected to yield a gravity high. Blakely (1985) postulates that Eureka Valley and Saline Valley were once a continuous valley that predates Pliocene sequences of basalt, implying there is a substantial amount of low density material underlying the Saline Range which would account for the anomaly. A residual anomaly gravity map was computed in Geosoft Oasis Montaj by differencing two raster datasets, one with all the available gravity data and the other excluding gravity data within the basin and also extending data from 1 km outside the basin margins (Figure 4.4). This method was developed by Mickus et al. (1991), and is the

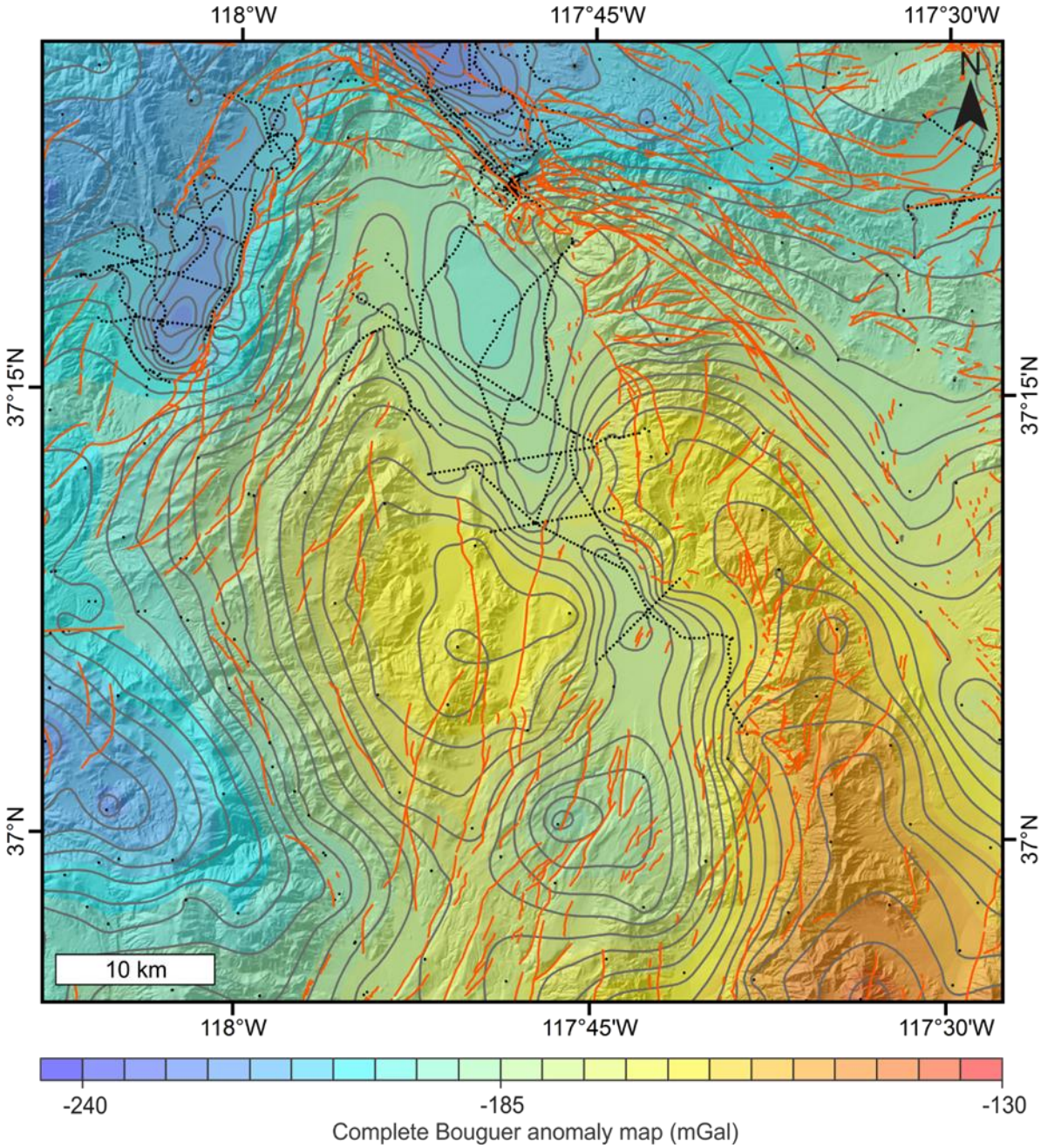

Figure 4.3. Bouguer gravity map of the Eureka Valley region. Gravity stations are shown in black and major faults shown in red.

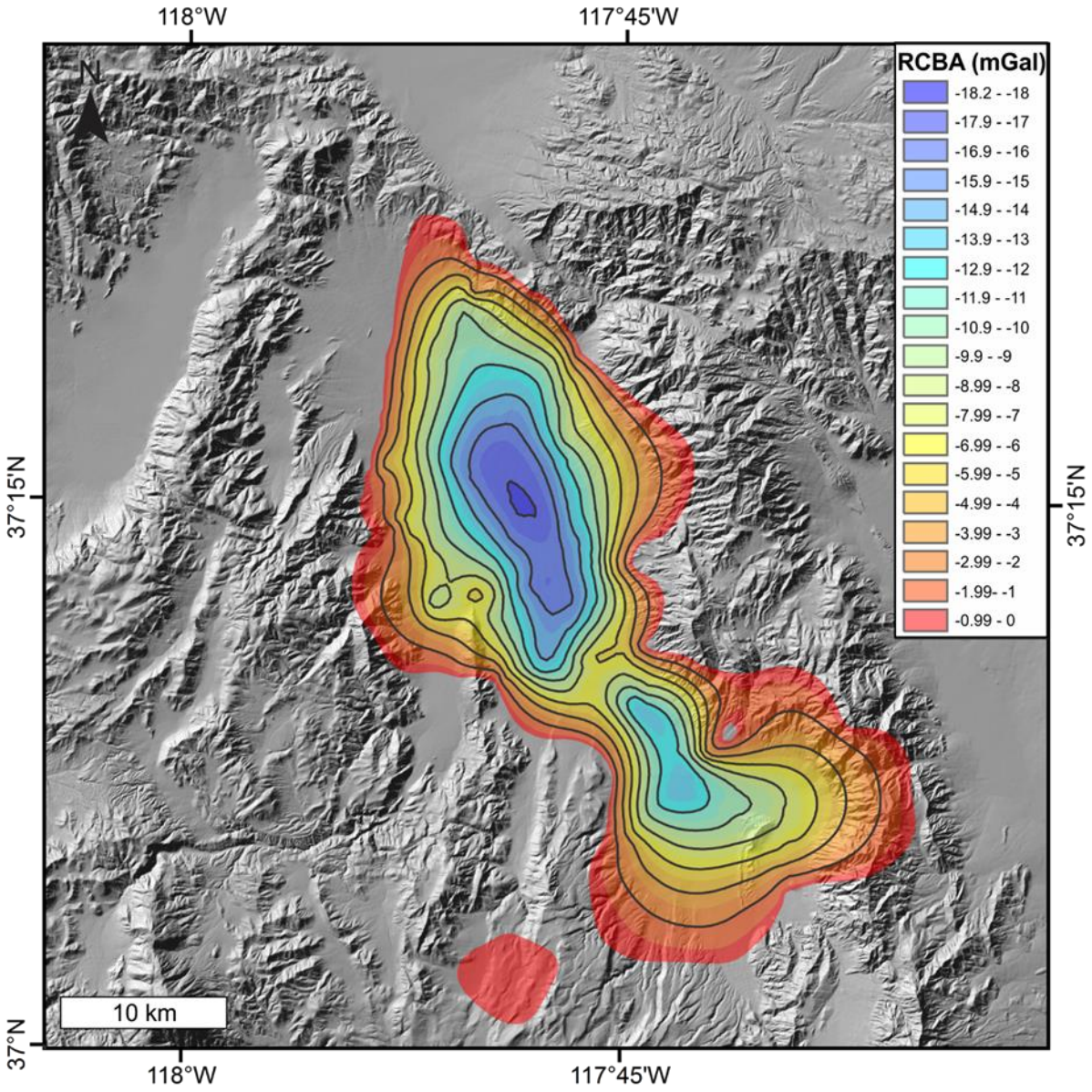

Figure 4.4. Residual Bouguer gravity anomaly map of Eureka Valley contoured at 2 mGal intervals.

minimum curvature technique, which eliminates the regional gravity trend and confines the gravity signature to the basin fill. The remaining gravity signal represents the gravitational effect of local geologic structures. To properly evaluate the residual anomaly map, knowledge of the regional features and stratigraphy is detrimental to deciding what an appropriate residual should represent. The residual gravity map (Figure 4.4) indicates that Eureka Valley is underlain by two gravity lows of -18 mGal in the north separated from a -14 mGal low in the south by a northeast trending high of -7 mGal that divides the basin into two sub-basins. The northern sub-basin, situated between the northern Inyo Mountains to the west and the Last Chance Range to the east, has a northwest trending maximum of -18.2 mGal. Within this sub-basin, 4 km to the south of the maximum anomaly is a northwest trending gravity low of -17 mGal. To the west and east of the maximum anomaly (~6.5 km on each side) produces a fairly smooth gradient to -3.1 mGal. In the northwest part of Eureka Valley, the gravity grades to 0 mGal roughly 4 km away from bedrock exposures. This could be due to sparse data in this region that do not adequately distinguish subsurface features or the presence of a pediment at the base of the Deep Springs Ridge. The central northwest trending high, 5 km to the southeast of the northern gravity low, ranges from -7 to -5 mGal and displays a saddle morphology. The southern sub-basin is divided into two regions, a northern north-west trending sub-basin, and a southern northeast sub-basin, both with -14 mGal values separated by 2 km by an amount of -12.6 mGal.

4.2 Depth Inversion

To effectively model the subsurface structures in the basin, a 3D depth to basement model was generated by inverting the residual Bouguer gravity map for depth. Inversion modeling was conducted in Geosoft Oasis Montaj GM-SYS 3D version 7.3 software, which applies the Parker-

Oldenburg algorithm (1974). This technique is an iterative procedure that applies a high-pass filter for calculating the spatial patterns of the anomalous perturbing body. The residual gravity data must be upward continued to the highest basin elevation to establish a common datum for interpretation (Cordell, 1973). This process reduces the residual gravity value and results in a maximum gravity signal loss of 2.12 mGal additionally reducing the depth of the basin.

Table 4.1. Density-depth values used in the gravity inversion modeling for Eureka Valley. (Modified from Scheirer, 2010).

Density-Depth Profile for Eureka Valley, CA	
Depth (km)	Density (g/cm^3)
0.0-0.2	2.0
0.2-0.6	2.1
0.6-1.2	2.3
>1.2	2.4

A preferred density of 2.67 g/cm^3 was used for bedrock, according to the parameters used by Hinze (2003). The porosity of sediments decreases with depth due to compaction, which results in an increase in density of basin fill with depth. To compensate for the lack of direct density measurements available in Eureka Valley, a density-depth profile (Table 4.1) which accommodates for density increasing with depth was modified from Blakely (1999) and Scheirer (2010) was used in the construction of the depth inversion (Figure 4.5a). Also, an effective density of 2.2 g/cm^3 for basin-fill model (Figure 4.5b) was generated and used as an additional end-member (Figure 4.5) in the 2D forward models used in many studies in the region (Pakiser and Kane, 1962, Pakiser et al., 1964). The deepest hole in the density-depth profile model is 694 meters and 979 meters in the effective density model. Depths in the effective density model

correspond with proposed depths of Eureka Valley determined by Blakely (1999).

The two depth to basement models correspond with major gravity trends in the residual Bouguer gravity map and were used as an upper and lower bounds in completing the two-dimensional forward models. The northern sub-basin previously defined in the residual displays maximum depths at 1.1 km and continues to show a northwest trend. The northwest area of Eureka Valley is not defined by the depth inversion model and is poorly defined by gravity data acquired in this survey and existing PACES stations. The northwest trending elongated southern sub-basin reaches a maximum depth of 900 meters.

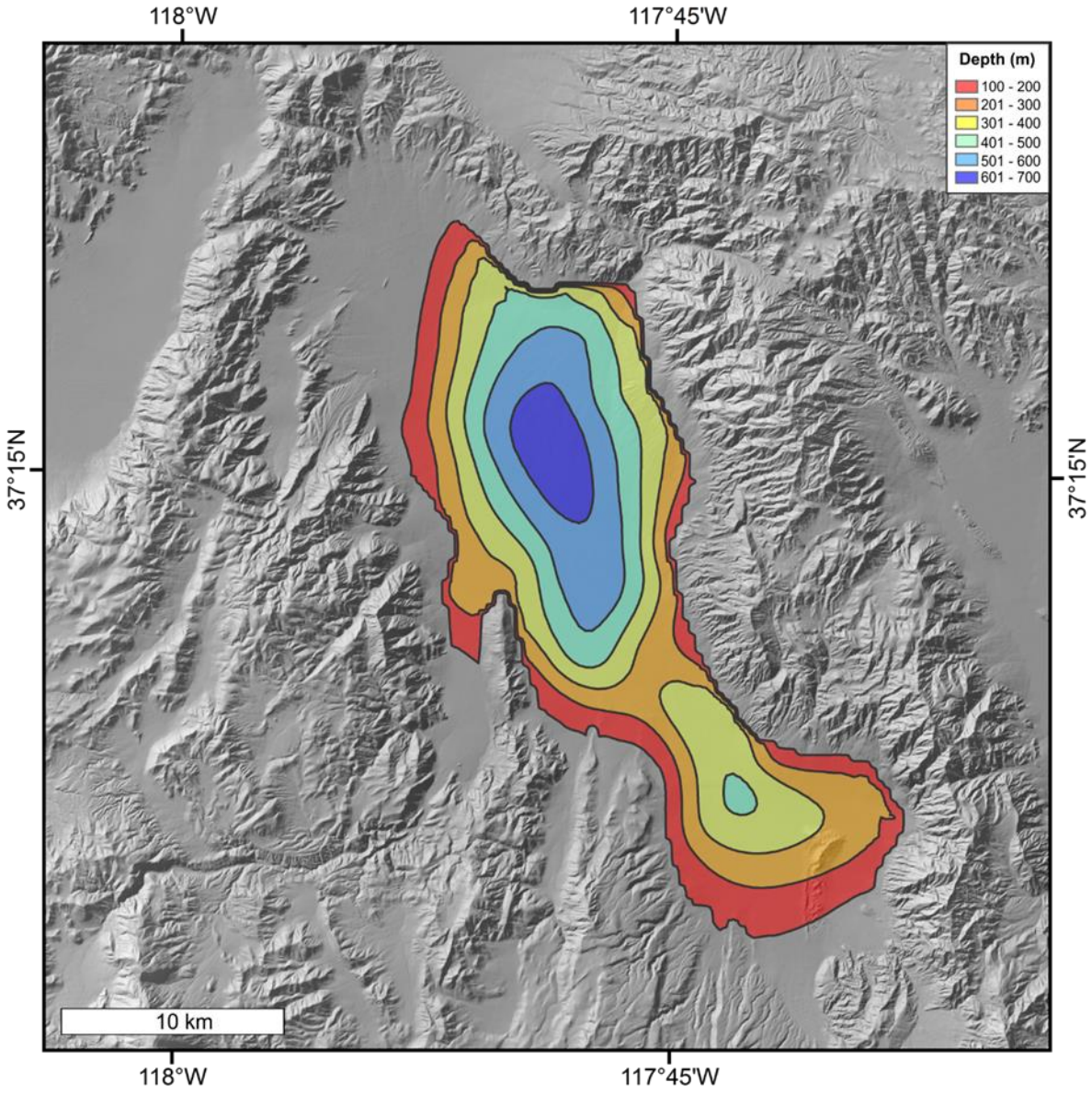

Figure 4.5a. Depth to basement of Eureka Valley applying the density-depth profile (Table 4.1) with 100 meter contours.

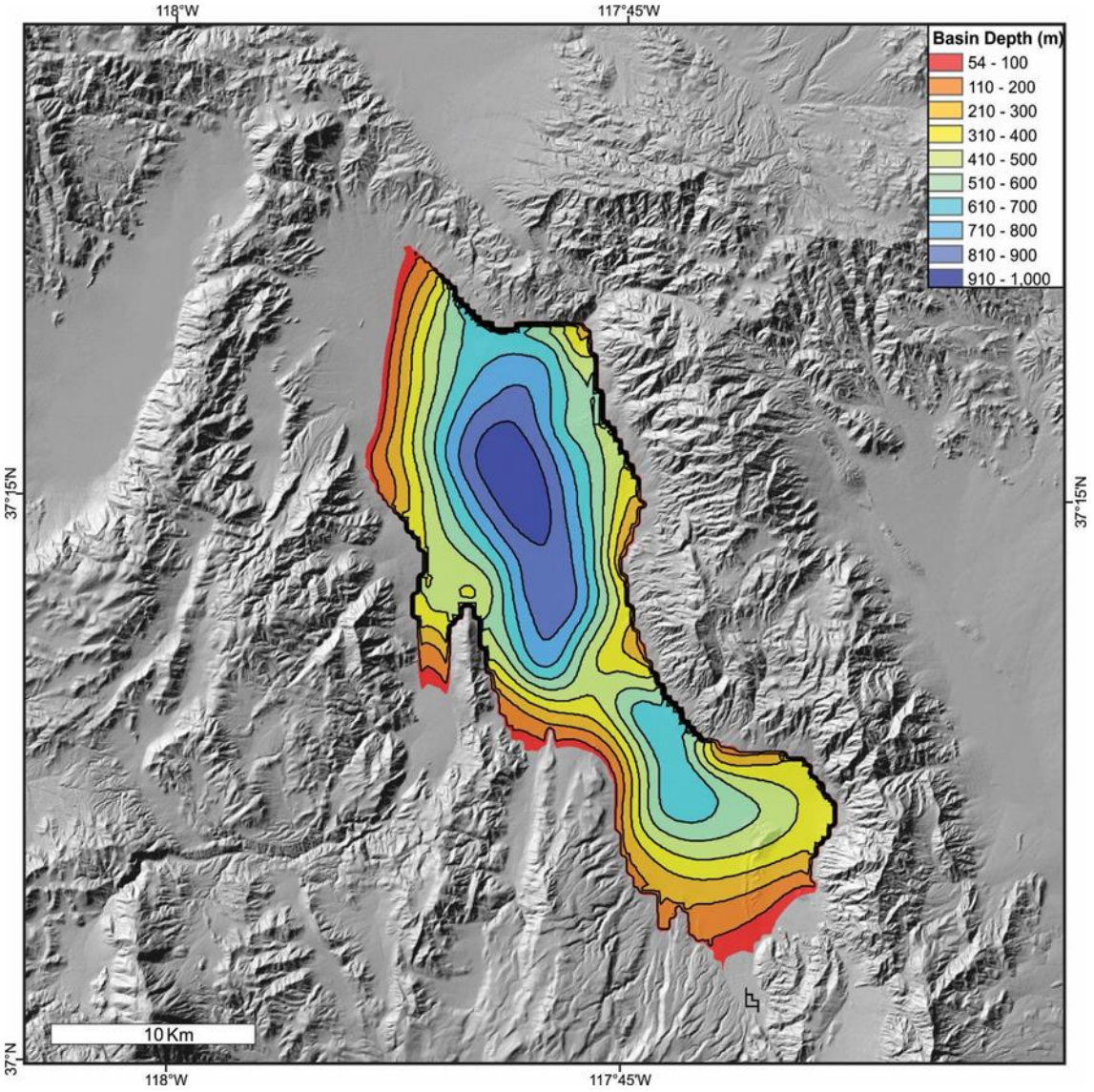

Figure 4.5b. Estimated depth to basement of Eureka Valley contoured at 100 meter intervals.

4.3 Subsurface Architecture

Identification of the local gravity gradients and corresponding depths derived from the inversion model allow the determination of the location and attitude of major subsurface features in the basin that lack visible surface preservation. Eureka Valley is partitioned into two structural domains, north and south, defined by the differences in gravity observations and the computation of the depth inversion (Figure 4.6) and this difference will be further examined in relation to the regional geologic structures. All positive gravity values have been excluded along with 0-50 meters from the depth inversion model. Both domains in Eureka Valley show similar character in anomalies, but differ in depth and size.

The northern domain occupies three-fifths of the basin and is characterized by a relatively smooth gradient and the deepest depth to basement in Eureka Valley. The residual gravity map nor the depth inversion extend to the region to the east of Soldier Pass Canyon, this could be attributed to the absence of adequate data in the region or an existing pediment surface. The boundary seen in both models, to the east of Solider Pass Canyon, is consistent with a north-northwest down to the southeast normal fault that serves as the bounding sub-basin fault. To the east of the Inyo Mountains, a high is present in both models and is consistent with the termination of a major topographic ridge to the south of the anomaly with north-northwest normal faults that flank the edges and is interpreted as a horst and graben structure. The main basement low is centered within the north domain, roughly 6-7 km on either side to the highlands and transitions to a steep gradient about 3 km away from the basin margins. The north and south boundaries of the depression correspond with the system of faults that emerge from the north of

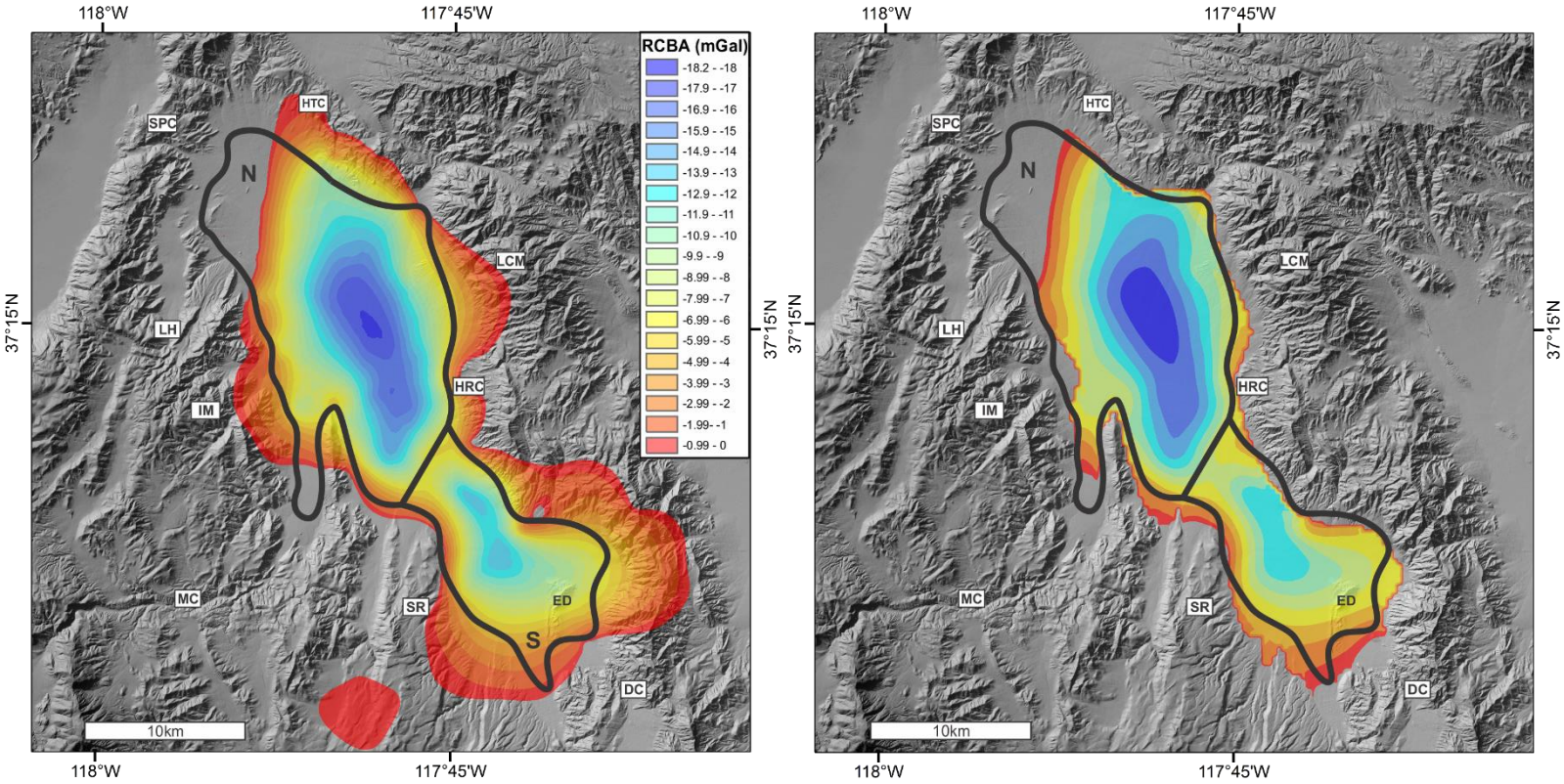

Figure 4.6. Two structural domains of Eureka Valley superimposed on the residual Bouguer gravity map (left) and the Isopach (right). N- Northern domain; S- Southern domain; SPC – Soldier Pass Canyon, HTC – Horse Thief Canyon, LCM- Last Chance Mountain, HRC- Hanging Rock Canyon, DC- Dedeckera Canyon, SR- Saline Range, MC- Marble Canyon, IM- Inyo Mountains, LH- Lime Hill

Saline Valley and cross-cut the northern Inyo Mountains. The northern basin bounding fault corresponds with a system of faults that runs parallel with Deep Springs Valley.

The southern domain, much like the north, displays an oblong deep depression and correspond to the trends seen in the RCBA but are less pronounced in the depth inversions (Figure 4.8). One major difference in the south is -2-4 mGal line extends into the surrounding range, which is interpreted by limited range control and a deficiency in data within the basin. The boundary between the two domains conforms to the system of northeast faults that cross the basin and link with structures bounding the Last Chance Range that creates a sub-surface ridge about 2 km wide.

4.4 Two-Dimensional Forward Models

The use of 2D forward models (Figure 4.7) provides additional means to test the viability of any structural interpretations and place estimations on the position and attitude of the subsurface architecture. Before construction, it is important to identify the key geologic features relative to this basin. Because no prior density contrast studies have been conducted, a density-depth profile (Table 4.1) characterizing the basin-fill was modified from regional studies (Saltus and Jachens, 1995; Blakely 1999; Scheirer, 2010) and resulted in densities between 2.0 and 2.4 g/cm^3. This model accommodates for density increasing with depth. Constant densities were used for Precambrian and Paleozoic metasedimentary rocks, and Cenozoic volcanic rocks (Table 4.2) and were assigned based on the values determined by Mueller (2017) and also in several regional studies (Pakiser and Kane, 1964; Saltus and Jachens, 1995; Blakely 1999; Scheirer, 2010; Dunn, 2015). The 2D forward models are limited to a single vertical plane and do not take into account the distribution of an anomalous, higher density body that could be adjacent to any

section and observed in the 3D model. In parts of the western study area, where Mesozoic plutons have intruded Paleozoic strata, density values can deviate and have slightly higher values near the Marble Canyon and Joshua Flat plutons. To diminish the impact of such density contrasts 2.75D modeling was used to account for contributing body. After the rock properties were defined, a first order structural model was proposed by building geologic cross-sections integrated with depths extracted from the 3D inversion and this was used as a template in the 2D models. Several iterations of the 2D model were fine-tuned until the gravity data showed a best fit to the model profile and aligned with the structural interpretation of Eureka Valley. Most structural data were limited to the highlands and range-front faults, and resolution at 300 meter spacing cannot determine dip values for faults in Eureka Valley and apparent dips were employed. The models were refined until an error of 0.4 or lower were obtained. Depth to basement within the 2D models were compared against the 3D inversion values and produced a maximum discrepancy of 14%, with the 2D models producing a slightly higher depth to basement value. A fence diagram (Figure 4.9) was produced, overlain on the geologic map, from the network of forward models to give a more 3D view of the basin morphology.

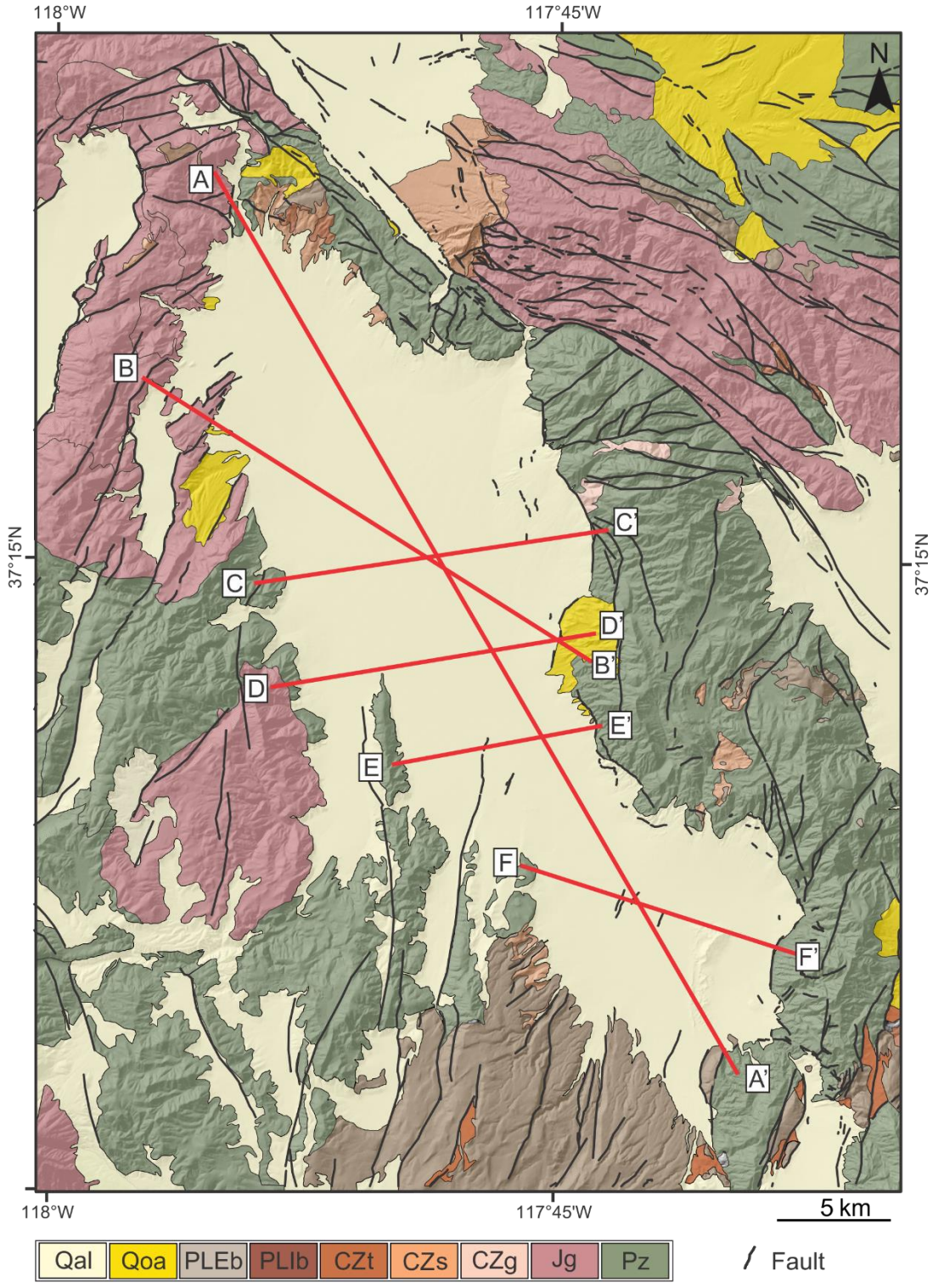

Figure 4.7. Geologic map of Eureka Valley with cross-sections for 2D forward models in red.

Table 4.2. Standardized rock properties for the lithologic units used in the 2D forward models.

Unit	Model density (g/cm^3)	Lithology
Qal	2.20	Quaternary alluvium and valley-fill deposits (0 - 1200 m)
Qoa	2.20	Quaternary alluvial fan and fluvial deposits (0 - ? m)
PLEb	2.90	Pliocene to Pleistocene basalt (0 - 400 m)
PLIb	2.90	Tertiary basalt (0 - 40 m)
CZt	2.40	Tertiary rhyolitic tuff (0 - 40 m)
CZs	2.40	Tertiary sedimentary rocks (0 - 50 m)
CZg	2.67	Miocene quartz monzonites of the Last Chance Range
Jg	2.70	Cretaceous and Jurassic quartz monzonites
Pz	2.70	Pre-Cambrian and Paleozoic meta-sedimentary rocks

Cross Section B-B'

Transect B-B' (Figure 4.8) trends west-northwest, with a strike of N58W, is situated at the northern end of the basin between the Deep Springs Ridge to the west and the Last Chance Range to the east. The western 3.6 km of this section is extrapolated data from the residual gravity map due to lack of access to this region. The remaining 23 km is collected data that ends in bedrock on the east and obliquely crosses the northern domain. The gravity gradient transitions from 0 mGal, on the west, to -18.6 mGal to -1.2 mGal in the far west. The cumulative vertical offset on all structures is 3074 m with fault dips of 60-65˚.

To the far west, minimal displacement is recorded west of the Paleozoic and Jurassic contact and depicts fault movement from the structures emanating from the Owens Valley fault system that are parallel to Deep Springs Valley. These structures from the far west are modeled

with 60-63˚ dips and cumulative vertical displacement of 735 m. To the east of the Paleozoic-Jurassic contact, the displacement estimate of five northeast to north-south trending, east dipping normal faults is 945 meters to basement. The eastern side of the northern sub-basin is controlled by north-northeast normal faults that can be traced from scarps in the northern Saline Range and cross the basin and drop-down to the northwest basement rocks with vertical offsets of 233, 191, 229, 265, and 105 meters from west to east. The Cenozoic sequence is not included in this section because there is no evidence of preservation in the area.

Cross Section C-C'

Transect C-C' (Figure 4.8) trends east-northeast, and extends 15.5 km across the width of the northern sub-basin from the Inyo Mountains to the base of the Last Chance Range, crossing the deepest part of the northern sub-basin at 950 meters depth. The structures depicted in this section illustrate the west and eastern margin of the northern sub-basin. These structures are modeled with apparent dips that are roughly 58-65˚ and consistent with the model line. The gravity gradient across the section is similar to B-B' transitioning from 0 mGal, on the west, to -18.1 mGals to -1 mGals in the east. Depth to basement within the model was compared against the 3D inversion and resulted in a maximum discrepancy of 7%.

The west and east basin margins are controlled by down to basement steep normal faults and produce a relatively symmetric graben. In the west, an array of north-south trending, down to the east normal faults control the down to basement steps to a depth of 906 meters. Focal mechanism solutions acquired from the U.S. Geological Survey Earthquakes Hazard Program Provided by National Earthquake Information Center (NEIC) for the M_W=4.7 and the M_W=4.2 earthquakes in Eureka Valley occurred southwest of Transect C determined north-south normal

fault with a minor component of strike-slip. The eastern extent of this section is modeled as several north-northeast down-to-the west normal faults with several surficial expressions of fault scarps from 1 to 5 meters high. The bounding highlands, on the east and west, were used to estimate vertical offset along this section due to lack of exposures of Cenozoic rocks.

Cross Section D-D'

Section D-D' (Figure 4.8) trends east-northeast and is situated roughly 6 km south and parallel to C-C' and is 14 km long. Cumulative vertical offset on all structures is about 3140 meters and faults are modeled with 57-63˚ dips. The gravity gradient, on the west, displays a -8 mGal low in between a -4 and -5 mGal high. The gradient smooths to -17 mGal about 4 km to the east and then reaches 0 mGal at the base of the Last Chance Range. The depth to basement in the 2D models was compared to the 3D inversion and reveals a minor discrepancy of 10 meters difference at the deepest point. The long-axis cross section was also compared and resulted in a 30 meter difference in depth to basement which is attributed to the location and change of trajectory of an overlapping N30E normal fault.

In the Inyo Mountains, the Marble Creek pluton bounds the western margin of the section with a sharp contact with Paleozoic metasedimentary rocks. The abrupt change in the gradient on the west corresponds to a topographic ridge about 500 meters south of the section and is modeled as a horst and graben structure. The structures to the east of the ridge defines the western boundary of the northern sub-basin and is modeled as three north-south trending normal faults with 60˚ dips that drop the basin down to the east. Vertical offsets measured on these structures are 92, 206 and 396 meters from west to east. A minor exposure of Cenozoic basalts are seen 100 meters south of the section at the foothills of the Last Chance Range and modeled with a density

of 2.9 g/cm^3. The east part of the profile is characterized by a system of down to the northwest normal faults and defines the division between the north and south sub-basins. On the east, four normal faults are modeled and yield estimated vertical displacement of 896 meters.

Cross Section E-E'

E-E' (Figure 4.8) stretches 14 km from a topographic ridge connected to the Inyo Mountains across the middle region of Eureka Valley into the Last Chance Range. This section trends north-northeast and intersects the saddle morphology shown by the gravity data. Total vertical offset along all structures is 3720 meters with assigned fault dips of 54-63˚. Most of the vertical displacement seen in this section is accommodated by a distributed array of normal faults and produces predicted basin depth of 750 meters. To accommodate for the profile ending on a ridge difference in topography was used to extend the section to the bounding highlands.

Gravity gradients on the far west end of the profile are modeled as three north-south trending down to the east normal faults that are included in the previous models. Farther east along the profile, an east-west trending gravity gradient remains at -5.7 mGals for 1.4 km. This is interpreted as the structural boundary between the north and south sub-basins and marks a change in orientation along strike to the west and east of the gravity high. To the west of the intrabasin high, an array of intra-basin normal faults that step the basin down to the west and result in a maximum depth of 750 meters. A series of north-northwest high angle structures bounding the highlands to the east contribute 200 meters of vertical offset. An 80 meter thick outcrop of Cenozoic basalt is localized to the east and inferred to pinch out heading west.

Cross Section F-F'

F-F' (Figure 4.8) trends north-west and is situated in the southern region of Eureka Valley and crosses the southern sub-basin. The western boundary is a topographic ridge bounding the Inyo Mountains and Saline Range and traverses south-east for 12 km to the south bounding Last Chance Range. Aggregate vertical offset along all structures in the southern domain is about 3635 m with assigned dips of 54 to 63˚. There is relatively little data coverage and therefore the southern section is poorly defined due to limited access within Death Valley National Park. Faults that cross the western region strike roughly north-northwest (N10W) and change orientation to northeast (N30E) to the southeast. Steep gravity gradients on the west are modeled as three down to the southeast structures that trend north-northwest and result in 224 m of vertical offset. An 80-300 meter thick sequence of basalt has been included within the southern cross-section due to the abundant exposure of basalt in Saline Range and in the Last Chance Range directly adjacent. Uncertainty remains in the stratigraphy of this region and this study follows Sternlof (1988) with modeling undifferentiated volcanic rocks. The sequence of sedimentary rocks below the basaltic flows is uncertain and exposures are laterally restricted excluded from the models.

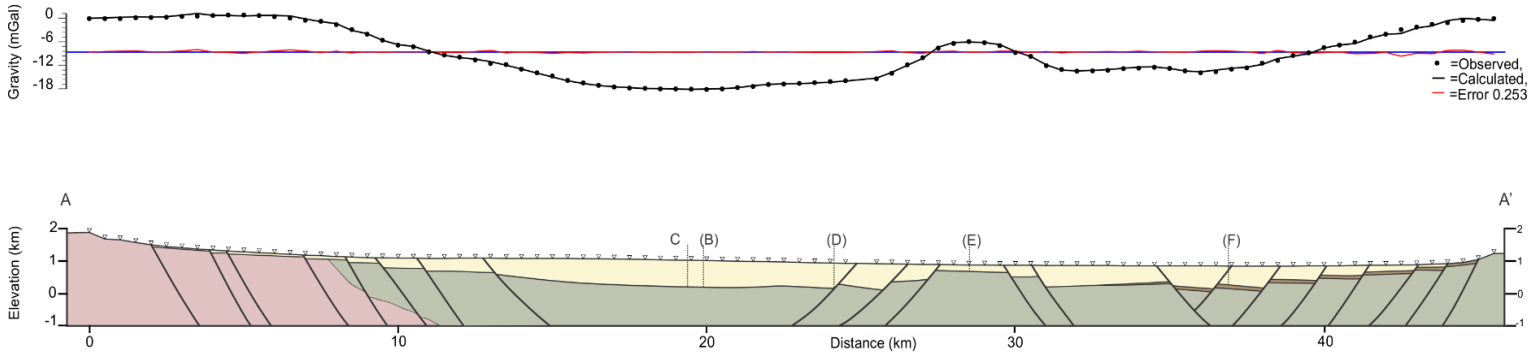

Figure 4.8. Two-dimensional geophysical models along section A-A' to F-F'. Profiles correspond cross-sections in Figure 4.7. Black dashed lines- profile crossing location.

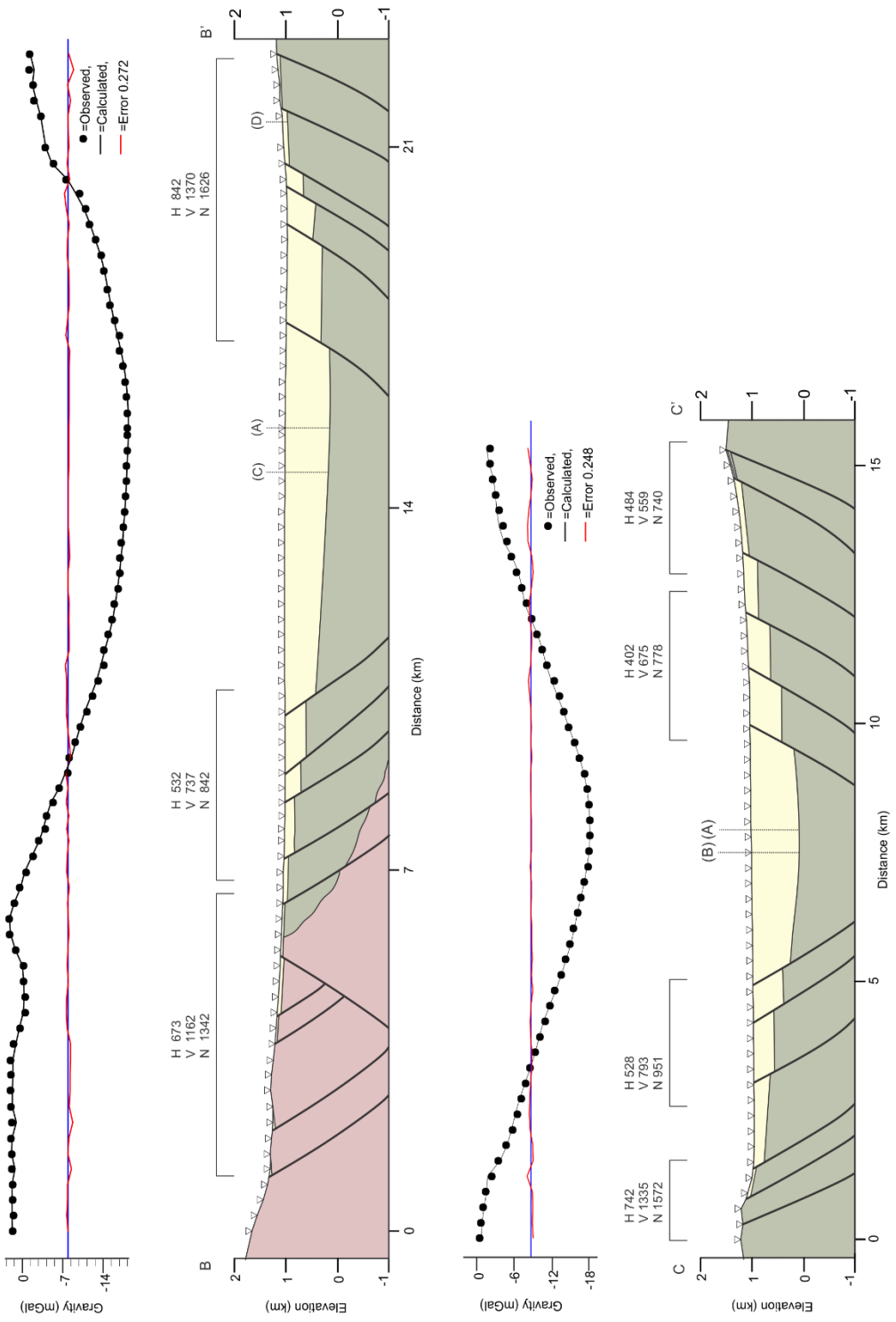

Figure 4.8. Continued.

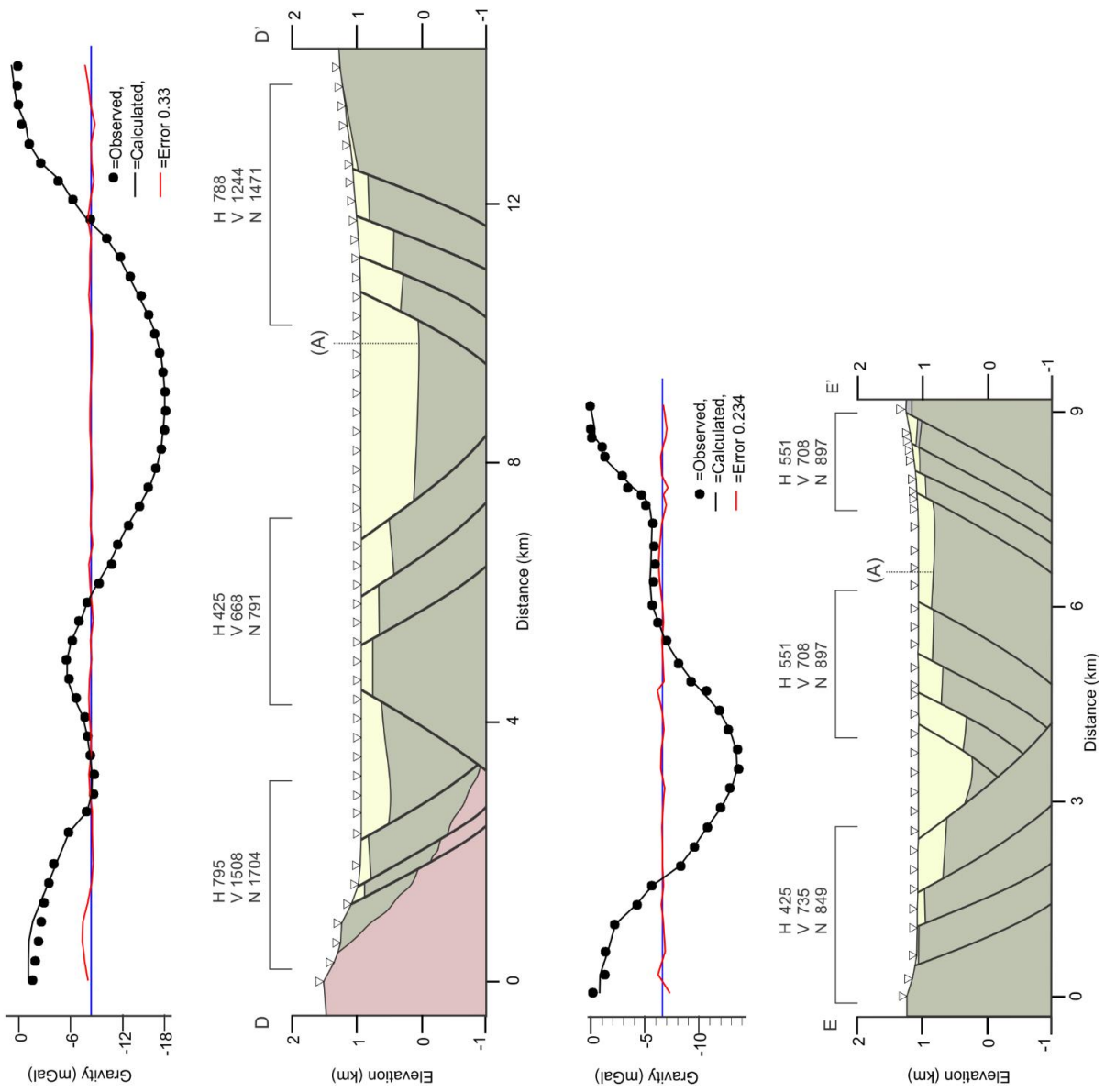

Figure 4.8. Continued.

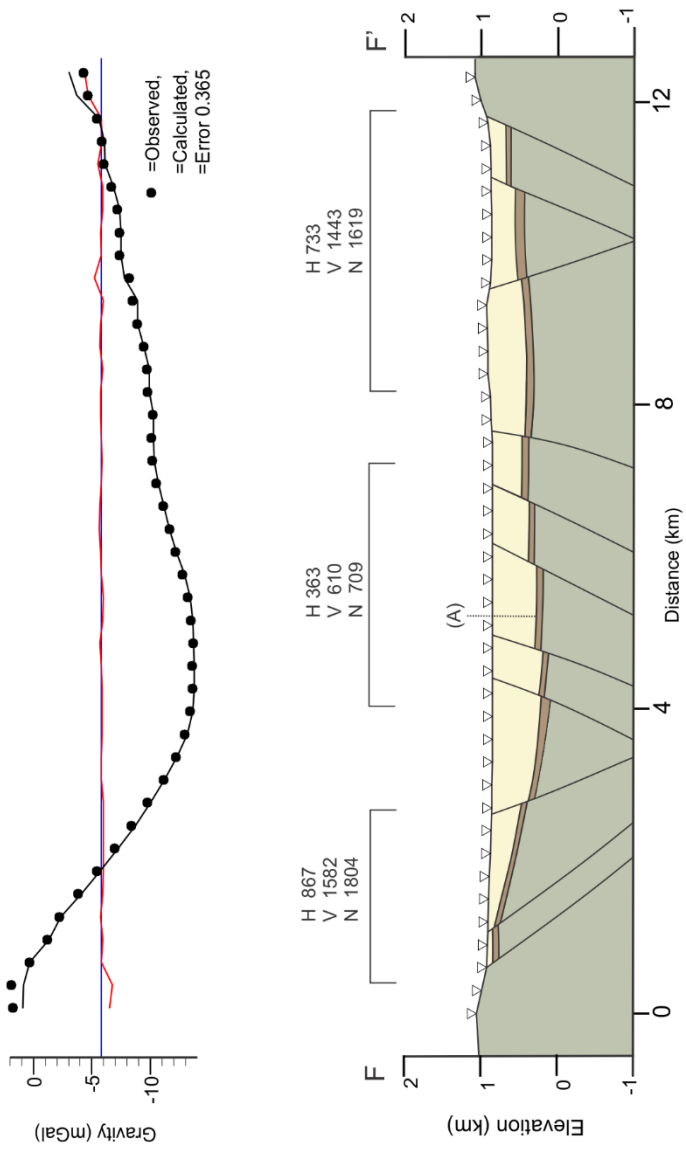

Figure 4.8. Continued.

Figure 4.9. Fence Diagram of two-dimensional forward profiles superimposed on a geologic map of Eureka Valley.

CHAPTER 5

BASIN FAULT MODEL AND DISPLACEMENT BUDGET

The vertical component of displacement for observed and inferred faults within the Eureka Valley fault system were incorporated with the established west-northwest extension direction to develop and analyze the following fault model for the basin. The regional extension direction, N65W, is well documented (Oldow, 1992, 2003; Oldow et al., 2008) and allows calculation of the horizontal magnitude of the system. For net slip calculations, the vertical component of displacement is incorporated for individual faults from the geometric relationship of geologic units and basin depths derived from the 3D model. Values for faults extending into the range were estimated from the difference in bounding topography. Net slip values show the dip-slip and strike-slip vectors associated with each fault. This is an important concern due to the change in strike of northeast trending faults that are predominantly dip-slip change orientation along a 45-60˚ arc, to north-northwest trending strike-slip dominated faults that will allow the determination of how displacement is partitioned on major faults in the basin. For this study, a long axis transect is constructed to assess the internal plausibility of the kinematic model.

5.1 Fault Model

A basin fault model (Figure 5.1) was constructed, based on observed and inferred faults from the gravity model, to determine the geometry of subsurface structures in Eureka Valley. Mapped faults for the area were provided by John S. Oldow and maps of Quaternary surficial features were obtained from the U.S. Geological Survey Seismicity in Eureka Valley, provided by the California Integrated Seismic Network via the U.S. Geological Survey Earthquake Hazards

Program website is active and has data recorded from 1980-2018 (SCEDC, 2013). The Bouguer gravity map, 3D depth inversion, and 2D forward models were used to identify local gravity gradients and evaluate the orientation of major subsurface structures. The complete and residual gravity maps and depth inversion display the trends of the gravity data and confine the areas of interest to determine magnitude of displacement. Two-dimensional models provide a detailed assessment of the gravity data along five transects from north to south in Eureka Valley. This provides a basis for determining the lateral continuity of structures within the basin and allows estimation of the vertical displacement vector for each fault strand. By determining the intersection of faults, we can determine how they interact with one another. From creating a map view of the area, we can then predict the consequences of the system.

Eureka Valley is characterized as an elongated extensional basin bound on the east by northeast oblique structures at the base of the Last Chance Range and north-south to north-northwest extensional faults that define the irregular western margin. The negative gravity anomalies (- mGal), depth inversion models and 2D forward models all show that Eureka Valley is segmented into a northern and southern domain, each of which contain a deep north-northwest trending sub-basin. The north-northeast trending structural high defined by the gravity gradients that internally dissect Eureka Valley is interpreted as a northeast trending normal intra-basin fault that serves as an accommodation zone and barrier segmenting the two regions with saddle like morphology.

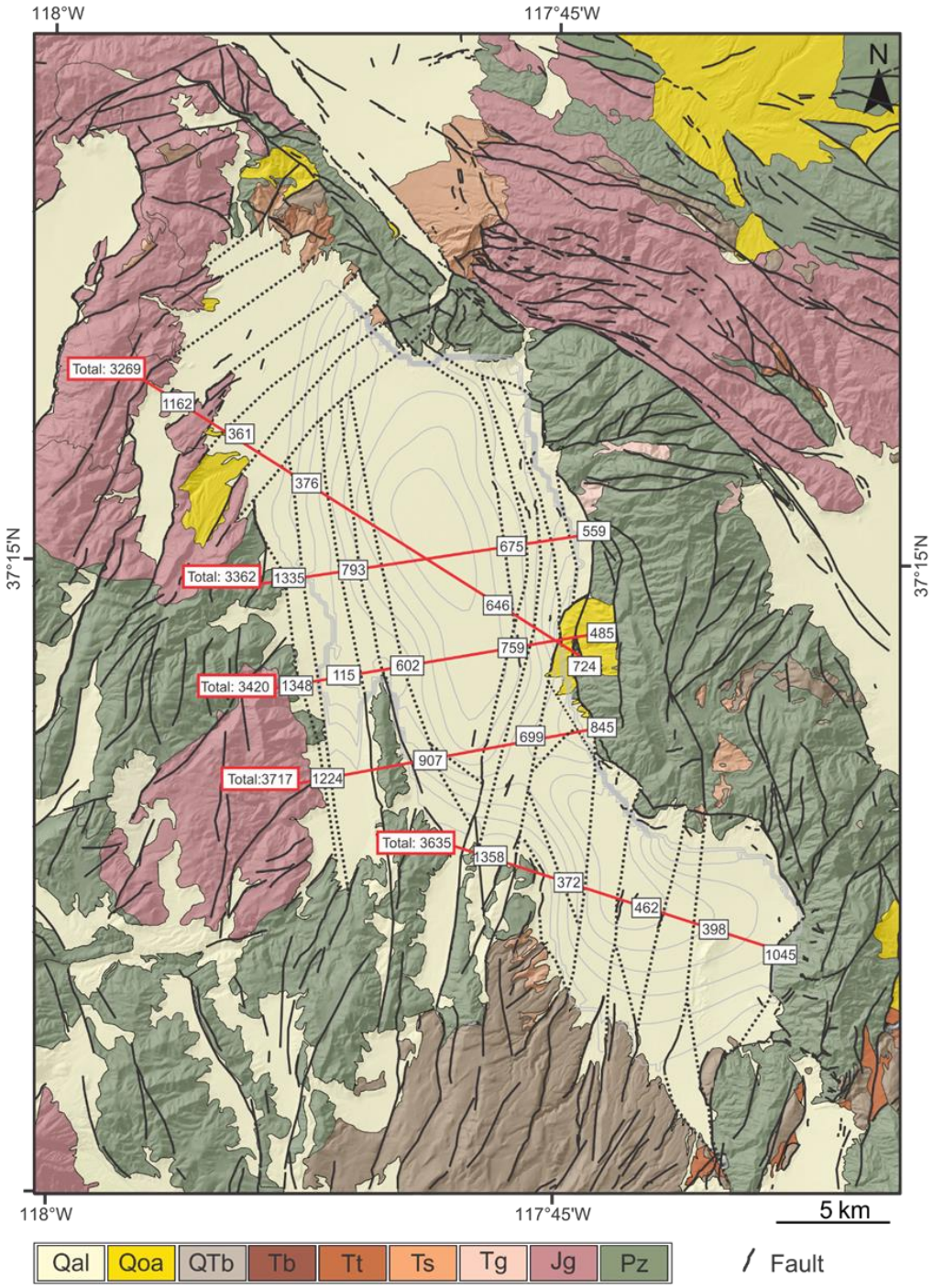

Figure 5.1. Vertical offsets measured for each two-dimensional forward model.

5.2 Displacement Component Determination

The magnitude of late Cenozoic displacement across individual faults, and subsequently the Eureka Valley fault system, can be quantified by the relative vertical offsets of late Pliocene to Pleistocene deposits in the surrounding range to basin depths extracted from the gravity model that correlate with the pre-deformation depositional surface. The pre-extensional datum established for Eureka Valley is an 11.5 Ma basalt flow lying unconformably on Jurassic monzonites of the Joshua Flat pluton on Chocolate Mountain. Restoration of structures to this reference datum at an elevation of 2240 m, allows a determination of a minimum estimate of the vertical component of displacement for the system. Despite the variation in lateral continuity of these rocks it is assumed that a very subdued topography existed at about 4 Ma, during the inception of basin formation and the younger deposits are indicative of multiple eruptions of volcanic rocks. Vertical offset estimates on structures in the system in the range as well as the basin bounding faults were obtained using a 10 m Digital Elevation Model and geospatially referenced images in Google Earth. Vertical offsets on basin bounding faults were restored to the established mid-Miocene datum where units were present. In areas where Cenozoic deposits are absent, the elevation of the Pre-Cenozoic rocks in the bounding highlands are interpreted to be the base of the section prior to erosion. Inter-basin faults with no surface expression were restored to the basin bounding fault elevation. The vertical offset values measured are minimum estimates due to the probability of unaccounted fault strands that were consolidated into fewer faults modeled.

For this study, geologic maps and gravity models were used to approximate the strike and dip of structures within the fault system. Structural data obtained from geologic maps were

primarily limited to the structures exposed in the highlands. The strike of structures emanating from the bounding highlands maintained trajectory, followed contours of the residual gravity map and some can be linked with few visible fault scarps. On structures where the dip was not known, normal faults within the valley were assigned dips of 60˚ and the apparent dip was calculated with respect to the strike of the 2D models. Cross-sections were made primarily along roads or walked paths that were available and were not always oriented in the extension direction. Two additional cross-sections were constructed by extracting data from the regional gravity map and oriented orthogonal to the trend of faults.

The vertical component of displacement can then be used to calculate the net slip and horizontal extension on each fault with respect to the extension direction, which will determine the ratio between strike-slip and dip-slip movement on each fault (Figure 5.2). First, each structure must be restored to a pre-deformation horizontal plane. Equation 1 computes the dip-slip component of a fault block projected to a horizontal plane using the vertical component of displacement and the estimated angle between the fault plane and the horizontal plane.

Equation 1:

$D_{HC} = \frac{V}{\tan(\theta)}$

θ= Dip angle of fault

V= Vertical component of displacement on fault

Horizontal extension can then be calculated using the dip-slip component resolved to the reference surface (previous calculation) and the acute angle between the established extension direction (Oldow et al., 2008; Biholar, 2011) and strike of the fault.

Equation 2:

$$HE = \frac{D_{HC}}{\sin(\phi)}$$

D_{HC}= Dip slip projected to the horizontal

ϕ = Angle between strike of fault and the extension direction ($\varepsilon 1$)

Net slip for each structure is calculated using the measured vertical component of displacement and the horizontal extension calculation in Equation 3. This calculation assumes that the displacement measured within the plane of the fault is parallel to the regional extension direction.

Equation 3:

$$NS = \sqrt{V^2 + HE^2}$$

V= Vertical component of displacement on fault

HE= Horizontal extension component

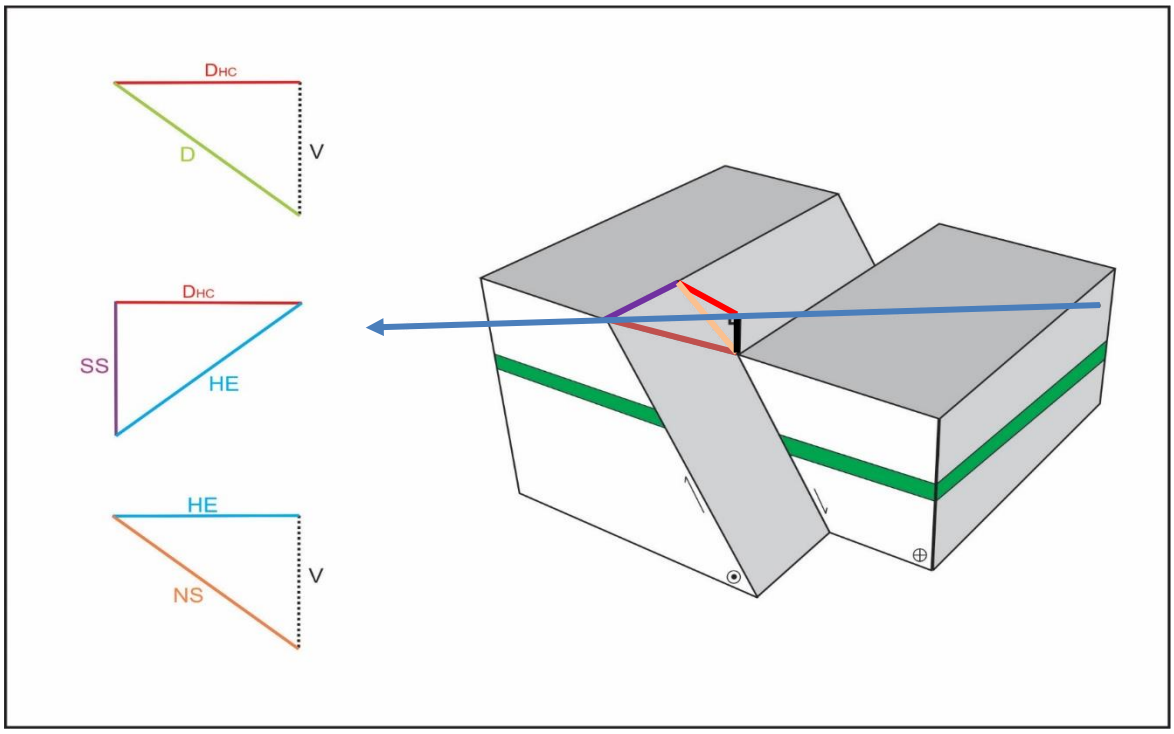

Figure 5.2. Block diagram modified from Biholar (2011) illustrating transtensional fault displacement. SS – Strike-slip component; D_{HC} – Dip-slip projected to the horizontal plane; HE – Horizontal extension component; NS – Net-slip component; V – Vertical displacement component.

5.3 Displacement Budget and Fault Evaluation

To determine a displacement budget (Figure 5.3) for this structurally complex system a rectilinear model of basin and range-bounding faults was constructed and the horizontal extension and net slip were derived for each structure. Kinematic analysis was done by creating a fault model that respected geometric constraints and adhered to the contours of the gravity models. Horizontal displacement was measured for all faults along three transects that trend east-west and two that trend northwest-southeast from north to south in Eureka Valley. Preferably transects would be oriented parallel with the extension direction, N65W, to reduce uncertainty in calculations but the study area had limited paths and an abundant distribution of sage brush. To

mitigate some of this uncertainty a section oriented along the basin axis that cross-cuts each transect was modeled and a depth comparison was done resulting in a maximum discrepancy of 50 meters.

Along the three parallel sections (C-C', D-D' and E-E') vertical offset increases from south to north although horizontal extension and net-slip remain constant. These sections occupy the central and northern section of the deepest sub-basin sections and are about 6 km apart from each other. The sections incorporate parallel structures, to the west and east, which transfer displacement to the north. Vertical offset values calculated on each cross-section differ from south to north. This variation could be attributed to the pre-extensional datum remaining constant along structures bounding the highlands to the west and the difference in topography of the valley floor, 1300-890 m, from north to south. Cumulative horizontal displacement (Figure 5.4) for these three sections produce compatible values with maximum difference of 48 m and support the internal consistency of the fault model represented in the north. Horizontal displacement values between C-C', D-D' and E-E' are 2156 m, 2108 m and 2102 m, respectively.

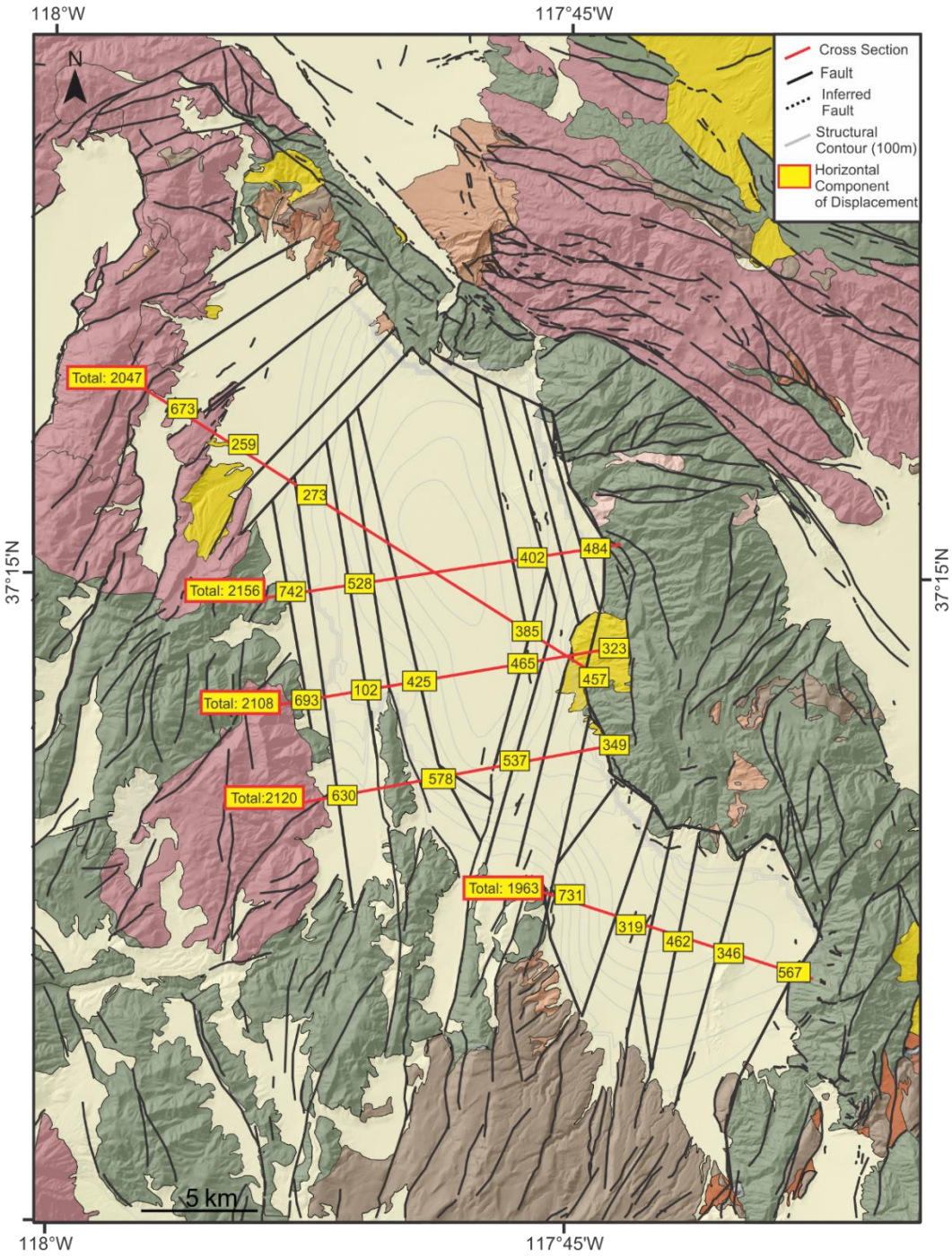

Figure 5.3. Fault map of Eureka Valley with measured horizontal component of displacement in yellow and cumulative values along each transect in yellow boxes with red outline.

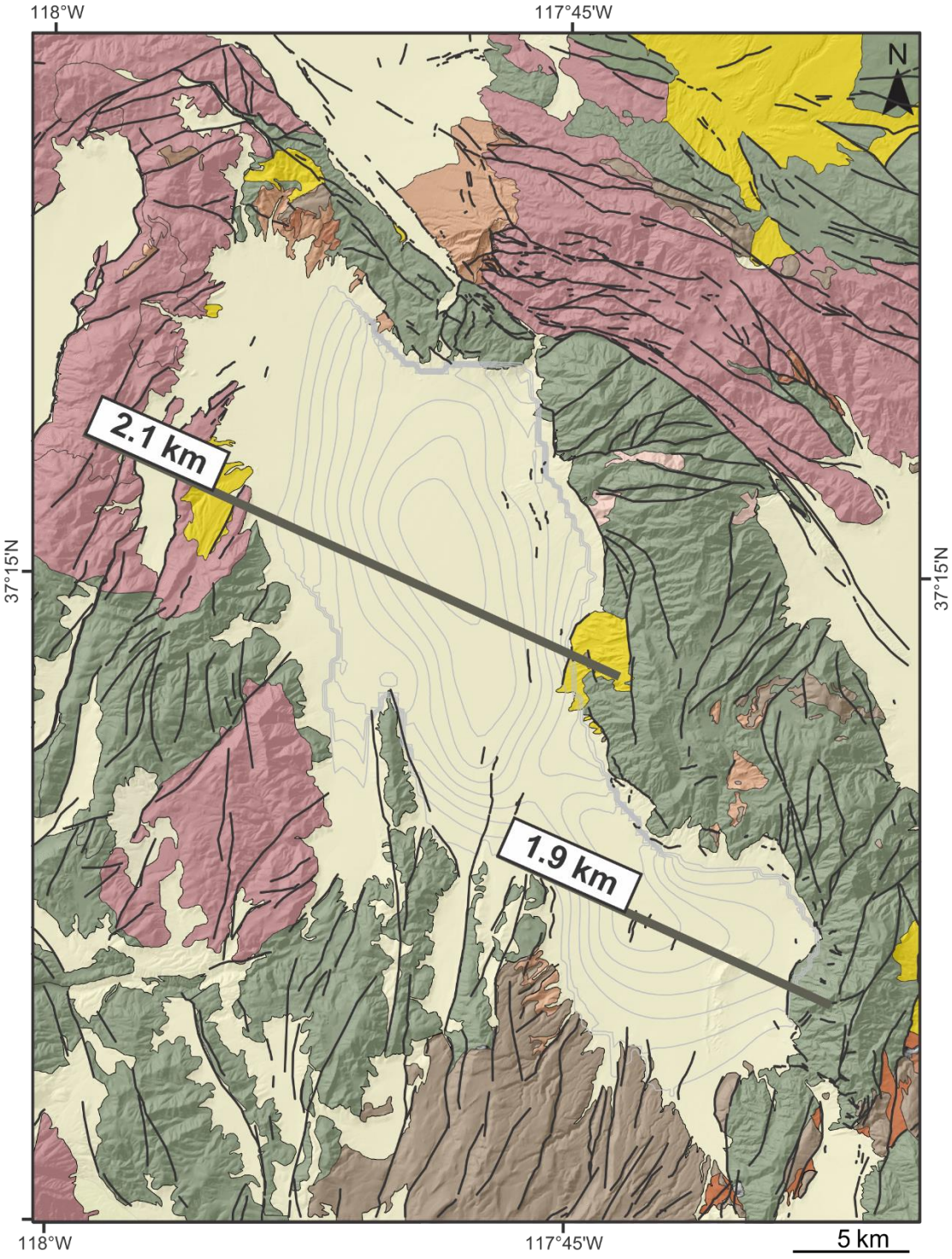

Figure 5.4. Simplified horizontal extension map for the north and south domains of Eureka Valley.

CHAPTER 6

DISCUSSION AND CONCLUSIONS

The Eureka Valley area of the northern part of the eastern California shear zone is characterized by a kinematically coordinated array of northeast-striking, northwest dipping normal faults that serve as a displacement transfer mechanism from the apex of the Saline Valley fault system north to the Furnace Creek - Fish Lake Valley fault system. The bulk of displacement transferred through Eureka Valley took place north of the 2D profiles from structures that are sub-parallel to the FC-FLV fault zone and to the east by the normal-oblique master fault that flanks the Last Chance Range.

During Pliocene to recent time, vertical offset in Eureka Valley, estimated by restoring structures to a late Miocene pre-deformational surface with geophysical modeling, produced two elongated northwest oriented sub-basins dissected by a subsurface topographical high. Maximum vertical offset in the north with a basement depth of 950 meters, this depression is a result of a basin ward step down of north-south extensional faults in the west and to the south and east by a system of north-northeast normal faults that tend to curve along strike and trend sub-parallel with structures exposed to the east. Maximum depths observed in the south are 675 meters and bound to the north by an array of extensional cross-valley faults and to the south by north-northwest structures that serve as a ramp emanating from the bounding range traversing north and northeast.

A fault displacement budget, with respect to the extension direction, allows for the trigonometric determination within the basin. Restoration to a pre-extensional datum yields minimum horizontal displacement for the northern and southern segments of about 2.1 and 1.9

km respectively. Displacement estimates are a minimum and uncertainty in these calculations could be due to the possibility of an open system.

Increase in right-lateral magnitude of displacement on the Furnace Creek - Fish Lake Valley fault zone from the mid-Pliocene to today is partially supplied by displacement transferred through Eureka Valley. The 4 km of displacement calculated in this study since 4 Ma results in an estimated slip rate of 1.0 mm/yr, or alternatively, 3.5 mm/yr since 1.4 Ma correlating to the age of the youngest volcanic succession. This result implies that the south to north increase in late Pleistocene slip-rate along Furnace Creek - Fish Lake Valley fault zone from Red Wall Canyon in Death Valley to Cucomungo Restraining Bend and, possibly north, is consistent with an increase in total magnitude of right-lateral displacement along this section of the fault zone from Pliocene to today.

REFERENCES

Argus, D.F., and Gordon, R.G., 1991, Current Sierra Nevada- North America motion from very long baseline interferometry: Implications for the kinematics of the western United States, Geology, v. 19, p. 1085-1088.

Bennett, R.A., Wernike, B.P., Neimi, N.A., Fredrich, A.M., and David, J.L., 2003, Contemporary strain rates in the northern Basin and Range from GPS data: Tectonics, v. 22, p. 3-1 – 3-31, doi: 10.1029/2001TC00135.

Blair, T.C., 2003, Features and origin of the giant Cucomungo Canyon alluvial fan, Eureka Valley, California: Special Paper 370: Extreme depositional environments: mega end members in geologic time, p. 105–126, doi: 10.1130/0-8137-2370-1.105.

Blakely, R.J., and Mckee, E.H., 1985, Subsurface structural features of the Saline Range and adjacent regions of eastern California as interpreted from isostatic residual gravity anomalies: Geology, v. 13, p. 781.

Blakely, R.J., Jachens, R.C., Calzia, J.P., and Langenheim, V.E., 1999, Cenozoic basins of the Death Valley extended terrane as reflected in regional-scale gravity anomalies: Special Paper 333: Cenozoic basins of the Death Valley region, p. 1–16, doi: 10.1130/0-8137-2333-7.1.

Burchfiel, B.C., Hodges, K.V., Royden, L.H., 1987, Geology of Panamint Valley – Saline Valley Pull-Apart System, California: Palinspastic Evidence for Low-Angle Geometry of a Neogene Range-Bounding Fault, Journal of Geophysical Research, v. 92, no. B10, p. 10,422-10,426.

Burchfiel, B.C. and Stewart, J.H., 1966, "Pull-apart" origin of the central segment of Death Valley, California: Bulletin of the Geological Society of America, v. 77, p. 439-442.

Cogbill, A.H., 1990, Gravity terrain corrections calculated using digital elevation models: Geophysics, v. 55, p. 102–106, doi: 10.1190/1.1442762.

Dalyrmple, G.B. 1963, Potassium-argon dates of some Cenozoic volcanic rocks of the Sierra Nevada, California: Geological Society of America Bulletin, v.74, p.379-390.

Dixon, T., Miller, M., Fariana., Wang, H., and Johnson, D. 2000, Present-day motion of the Sierra Nevada block and some tectonic implications for the Basin and Range province, North American Cordillera: Tectonics, v. 19, p. 1-24, doi: 10.1029/1998TC001088.

Dokka, R.K. and Travis, J., 1990, Role of the Eastern California shear zone in accommodating Pacific-North American plate motion: Geophysical Research Letters, v. 17, no. 9, p. 1323-1326.

Dunn, S.B., Oldow, J.S., Mueller, N.J., 2015, Late Cenozoic displacement transfer in the eastern Sylvania Mountain fault system and Lida Valley pull-apart basin, southwestern Nevada, based on three-dimensional gravity depth inversion and forward models: Geosphere v. 11, no. 5, p. 1565-1589, doi:1130/GEOS1151.1.

Frankel, K. L., 2007a, Cosmogenic 10Be and 36Cl geochronology of offset alluvial fans along the northern Death Valley fault zone: Implications for transient strain in the eastern California shear zone: Journal of Geophysical Research, v. 112, p. B06407, doi: 10.1029/2006/JB004350.

Frankel, K. L., Dolan, J. F., Finkel, R. C., Owen, L., and Hoeft, J. S., 2007b, Spatial variations in slip rate along the Death Valley-Fish Lake Valley fault system determined from LiDAR topographic data and cosmogenic 10Be geochronology: Geophysical Research Letters, v. 34, p. L18303, doi: 10.1029/2007/GL030549.

Healey, D., 1970, Gravity surveys in the California portion of the Kingman quadrangle: Open-File Report, doi: 10.3133/ofr70158.

Hildebrand, T.G., Briesacher, A., Flanagan, G., Hinze, W.J., Hittelman, A.M., Keller, G.R., Kucks, R.P., Plouff, D., Roest, W., Seeley, J., Smith, D.A., and Webring, M., 2002, Rationale and Operational Plan to Upgrade the U.S. Gravity Database: U.S. Geological Survey Open-File Report 02-463, 12p.

Hinze, W. J., Aiken, C., Brozena, J., Coakley, B., Dater, D., Flanagan, G., & Kucks, R. (2005). New standards for reducing gravity data: The North American gravity database. Geophysics, 70(4), J25-J32.

Holom, D.I., and J.S. Oldow, 2007, Gravity reduction spreadsheet to calculate the Bouguer anomaly using standardized methods and constants: Geosphere 3, p. 86-90.

Gourmelen, N., Dixon, T.H., Amelung, G.S.,2010, Acceleration and evolution of faults: An example from the Hunter Mountain-Panamint Valley fault zone, Eastern California, Earth and Planetary Science Letters 301 (2011) 337-344 doi: 10.1016/j.epsl.2010.11.016.

Gravity and basin-depth maps of the Basin and Range Province, Western United States, 1995, doi: 10.3133/gp1012.

Kane, M.F., and Pakiser, L.C., 1961, Geophysical Study of Subsurface Structure in Southern Owens Valley, California: Geophysics, v. 26, p. 12–26, doi: 10.1190/1.1438835.

Katopody, D.T., 2018, Extensional and Accretionary Tectonics of Western North America: Examples from the Southern Walker Lane and Northwestern Washington State: The University of Texas at Dallas.

Knott, J., Sarnawojcicki, A., Machette, M., and Klinger, R., 2005, Upper Neogene stratigraphy and tectonics of Death Valley — a review: Earth-Science Reviews, v. 73, p. 245–270, doi: 10.1016/j.earscirev.2005.07.004.

Knott, J.R., Sarna-Wojcicki, A.M., Meyer, C.E., Tinsley, J.C., Wells, S.G., and Wan, E., 1999, Late Cenozoic stratigraphy and tephrochronology of the western Black Mountains piedmont, Death Valley, California: Implications for the tectonic development of Death Valley: Special Paper 333: Cenozoic basins of the Death Valley region, p. 345–366, doi: 10.1130/0-8137-2333-7.345.

Larson, N.W., 1979, Chronology of Late Cenozoic basaltic volcanism; the tectonic implications along a segment of the Sierra Nevada and Basin and Range Province County. Bringham Young University, PhD dissertation. P.95.

Lee, J., Rubin, C. M., & Calvert, A. 2001. Quaternary faulting history along the Deep Springs fault, California. GSA Bulletin, 113(7), 855-869.

Lee, J., Stockli, D.F., Owen, L.A., Finkel, R.C., and Kislitsyn, R., 2009a, Exhumation of the Inyo Mountains, California: Implications for the timing of extension along the western boundary of the Basin and Range Province and distribution of dextral fault slip rates across the eastern California shear zone. Tectonics, v. 28, TC1001, doi:10.1029/2008TC002295.

Litinsky, V. A. (1989). Concept of effective density: Key to gravity depth determinations for sedimentary basins. Geophysics, 54(11), 1474-1482.

McKee, E. H., & Nash, D. B. (1967). Potassium-argon ages of granitic rocks in the Inyo batholith, east-central California. Geological Society of America Bulletin, 78(5), 669-680.

McKee, E. H., & Nelson, C. A. (1967). Geologic map of the Soldier Pass quadrangle, California and Nevada (No. 654).

McKee, E.H., 1968, Age and rate of movement on the northern part of the Death Valley – Furnace Creek fault zone, California: Geological Society of America Bulletin, v. 79, p. 509-512.

Mickus, K.L., C.L.V. Aiken, and W.D. Kennedy, 1991, Regional-residual gravity anomaly separation using the minimum-curvature technique: Geophysics 56, no. 2, p. 279-283.

Mouslopoulou, V., Nicol, A., Little, T., and Walsh, J., 2007, Displacement transfer between intersecting regional strike-slip and extensional fault systems: Journal of Structural Geology, v. 29, p. 100–116, doi: 10.1016/j.jsg.2006.08.002.

Mueller, N., and Oldow, J.S., 2017, Pliocene changes in kinematics and long-term geologic slip rates along the Furnace Creek – Fish Lake Valley fault zone, California and Nevada: Geological Society of America Abstracts with Programs, v.49, no. 6, 385-21.

Mueller, N. J. and Oldow, J.S., 2018, Pliocene to Holosene Displacement Budget Along the Fish Lake Valley Fault Zone, Eastern California - Southwestern Nevada: American Association of Petroleum Geologists.

Oldenburg, D.W., 1974, The inversion and interpretation of gravity anomalies: Geophysics 39, p. 526-536.

Oldow, J.S., 1992, Late Cenozoic displacement partitioning in the northwestern Great Basin: Structure Tectonics and Mineralization of the Walker Lane, Stewart, J., ed., Walker Lane Symposium Proceedings Volume, Geological Society of Nevada, Reno, NV, p. 17-52.

Oldow, J.S., 2003, Active transtensional boundary zone between the western Great Basin and Sierra Nevada block, western U.S. Cordillera: Geological Society of America, Geology, v. 31, no. 12, p. 1033-1036.

Oldow, J.S., G. Kohler, and R.A. Donelick, 1994, Late Cenozoic extensional transfer in the Walker Lane strike-slip belt, Nevada: Geology, v. 22, p. 637-640.

Oldow, J.S., J.W. Geissman, and D.F. Stockli, 2008, Evolution and strain reorganization within late Neogene structural step-overs linking the central Walker Lane and northern Eastern California shear zone, western Great Basin: International Geology Review, v. 50, p. 1-21.

Oldow, J.S., E.A. Elias, L. Ferranti, W.C. McClelland, and W.C. McIntosh, 2009, Late Miocene to Pliocene synextensional deposition in fault-bounded basins within the upper plate of the western Silver Peak-Lone Mountain extensional complex, west-central Nevada: Geological Society of America Special Paper 447: Late Cenozoic Structure and Evolution of the Great Basin-Sierra Nevada Transition, p. 275-312.

Oswald, J.A., and Wesnousky, S.G., 2002, Neotectonics and Quaternary geology of the Hunter Mountain fault zone and Saline Valley region, southeastern California: Geomorphology, v. 42, p. 255–278, doi: 10.1016/s0169-555x(01)00089-7.

Pakiser, L., Kane, M.F., and Jackson, W., 1964, Structural geology and volcanism of Owens Valley region, California -- a geophysical study: Professional Paper, doi: 10.3133/pp438.

Pan American Center for Earth and Environmental Studies (PACES), 2005, The University of Texas at El Paso, Gravity database of the United States: http://www.research.utep.edu.

Peltzer, G., and Rosen, P., 1995, Surface Displacement of the 17 May 1993 Eureka Valley, California, Earthquake Observed by SAR Interferometry: Science, v. 268, p. 1333–1336, doi: 10.1126/science.268.5215.1333.

Reheis, M. C., 1992, Geologic map of late Cenozoic deposits and faults in parts of the Soldier Pass and Magruder Mountain 15' quadrangles, Inyo and Mono counties, California, and Esmeralda County, Nevada: U.S. Geological Survey Miscellaneous Investigations Series Map I-2268, p. scale 1:24,000.

Reheis, M. C., and Dixon, T. H., 1996, Kinematics of the Eastern California shear zone: Evidence for slip transfer from Owens and Saline Valley fault zones to Fish Lake Valley fault zone: Geology, v. 24, p. 575-575.

Reheis, M. C., and Sawyer, T. L., 1997, Late Cenozoic history and slip rates of the Fish Lake Valley, Emigrant Peak, and Deep Springs fault zones, Nevada and California: Geological Society of America Bulletin, v. 109, p. 280-299.

Ross, D., 1970, Pegmatitic trachyandesite plugs and associated volcanic rocks in the Saline Range-Inyo Mountains region, California: U.S. Geological Survey Professional Paper, doi: 10.3133/pp614d.

Saltus, R.W., and Jachens, R.C., 1995, Gravity and basin-depth Maps of the Basin and Range Province, Western United States: U.S. Geological Survey Map GP-1012, scale 1:2,500,00.

SCEDC (2013): Southern California Earthquake Center. Caltech.Dataset. doi:10.7909/C3WD3xH1.

Scheirer, D.S., Sweetkind, D.S., and Miller, J.J., 2010, Multiple phases of basin formation along the Stateline fault system in the Pahrump and Mesquite Valleys, Nevada and California: Geosphere, v. 6, p. 93–129, doi: 10.1130/ges00520.1.

Sternlof, K.S., 1988, Structural style and kinematic history of the active Panamint – Saline extensional system, Inyo county, California. MIT MS Thesis.

Stockli, D.F., Dumitru, T.A., Mcwilliams, M.O., and Farley, K.A., 2003, Cenozoic tectonic evolution of the White Mountains, California and Nevada: Geological Society of America Bulletin, v. 115, p. 788–816, doi: 10.1130/0016-7606(2003)115<0788:cteotw>2.0.co;2.piedmont, Death Valley, California: Implications for the tectonic development of Death Valley: Special Paper 333: Cenozoic basins of the Death Valley region, p. 345–366, doi: 10.1130/0-8137-2333-7.34.

BIOGRAPHICAL SKETCH

Lauren Landreneau was born in Houston, Texas and grew up in south Louisiana and north Florida. She received her Bachelor of Science in Geosciences in December 2016 from The University of Texas at Dallas. Lauren fast-tracked into the master's program in August 2016 at The University of Texas at Dallas and continued her graduate studies until spring of 2019.

CURRICULUM VITAE

Lauren A. Landreneau

800 W Campbell Rd, Richardson, Texas 75080
University of Texas at Dallas, Department of Geosciences, ROC 21

Education

Master of Science in Geosciences
The University of Texas at Dallas
Fall 2016 – Spring 2019

Bachelor of Science in Geosciences
The University of Texas at Dallas
Spring 2015 – Fall 2016

Awards

Dallas Geological Society Scholarship Summer 2016

Pioneer Natural Resources Scholarship Fall 2016 – Fall 2018